creative commons
COMMONS DEED

저작자표시-비영리-변경금지 2.0 대한민국

이용자는 아래의 조건을 따르는 경우에 한하여 자유롭게

- 이 저작물을 복제, 배포, 전송, 전시, 공연 및 방송할 수 있습니다.

다음과 같은 조건을 따라야 합니다:

저작자표시. 귀하는 원저작자를 표시하여야 합니다.

비영리. 귀하는 이 저작물을 영리 목적으로 이용할 수 없습니다.

변경금지. 귀하는 이 저작물을 개작, 변형 또는 가공할 수 없습니다.

- 귀하는, 이 저작물의 재이용이나 배포의 경우, 이 저작물에 적용된 이용허락조건을 명확하게 나타내어야 합니다.
- 저작권자로부터 별도의 허가를 받으면 이러한 조건들은 적용되지 않습니다.

저작권법에 따른 이용자의 권리는 위의 내용에 의하여 영향을 받지 않습니다.

이것은 이용허락규약(Legal Code)을 이해하기 쉽게 요약한 것입니다.

Disclaimer

dCollection

A Dissertation for the Degree of Doctor of Philosophy

Hepatotoxic Mechanisms of Ephedrine and Dihydroceramide through Impaired Autophagy

에페드린과 디히드로세라마이드로 유도된 오토파지 손상에 의한 간 독성 기전

By

Ah Young Lee

August 2018

Department of Veterinary Pathobiology and Preventive Medicine,

Graduate School of Seoul National University

ABSTRACT

Hepatotoxic Mechanisms of Ephedrine and Dihydroceramide through Impaired Autophagy

Ah Young Lee

Department of Veterinary Pathobiology and Preventive Medicine,

Graduate School of Seoul National University

Supervisor : Kyung-Sun Kang, D.V.M., Ph.D.

Non-alcoholic fatty liver disease (NAFLD) is an increasingly common chronic liver disease worldwide. The pathogenic mechanisms underlying the progression of NAFLD are not fully understood. Therefore, the aims of this study are to assess the relationship between oxidative stress and autophagy in human hepatocytes during NAFLD. Autophagy also is an adaptive response under stressful

conditions, and basal level of autophagy ensures the physiological turnover of old and damaged organelles. Recent studies have shown that autophagy plays a role in NAFLD. Thus, autophagic pathway can be a novel therapeutic target for liver disease.

The herb *Ephedra sinica* (also known as Chinese ephedra or Ma Huang), used in traditional Chinese medicine, contains alkaloids identical to ephedrine and pseudoephedrine as its principal active constituents. Ephedrine is known as an effective diet component. However, recent studies have reported that ephedrine has various side effects in the cardiovascular and nervous systems. In addition, herbal Ephedra, a plant containing many pharmacologically active alkaloids, principally ephedrine, has been reported to cause acute hepatitis. Many studies reported clinical cases, however, the cellular mechanism of liver toxicity by ephedrine remains unknown. This study investigated hepatotoxicity and key regulation of mitophagy in ephedrine-treated LX-2 cells. Ephedrine triggered mitochondrial oxidative stress and depolarization. Mitochondrial swelling and autolysosome were observed in ephedrine treated cells. Ephedrine also inhibited mitochondrial biogenesis, and the mitochondrial copy number was decreased. Parkin siRNA recovered the ephedrine-induced mitochondrial damage. Excessive mitophagy lead to cell death through imbalance of autophagic flux. Moreover, antioxidants and reducing Parkin level could serve as therapeutic targets for ephedrine-induced hepatotoxicity.

Sphingolipids are a family of lipids that play essential roles as critical regulators in metabolic disorders. Some sphingolipids are known key factors in metabolic dysfunction. However, the precise effect of dihydroceramide on NAFLD

remains unknown. Here, these results report how dihydroceramide in autophagosome accumulation activates fibrogenesis in human liver Chang cells treated with free fatty acids (FFA). According to LC/MS lipid profiling, FFA increased the levels of sphingolipids and triacylglycerol (TG). To demonstrate the potential role of dihydroceramide metabolism in autophagy, several sphingolipid synthesis inhibitors were used. Increased dihydroceramide led to impairment of autophagic flux, resulting in increased TG storage in lipid droplets (LD) and upregulated expression of fibrosis markers. Hepatic stellate cells (HSCs, LX-2 cells) were co-cultured with Chang cells to assess the potential fibrogenic response to dihydroceramide, Treatment with rapamycin recovered autophagic flux in Chang cells and fibrogenesis in the co-culture system. These results identified a critical function of dihydroceramide metabolism in autophagy. It could play an important role in the progression of NAFLD associated with lipid over-accumulation. Therefore, preventing autophagic flux by regulating dihydroceramide could be a potential strategic approach for providing therapy for NAFLD.

Taken together, these findings demonstrate that oxidative stress induces hepatic toxicity through impairment of autophagy. Also, increased dihydroceramide induces fibrosis response through impaired autophagic flux. Consequently, this study evaluated hepatotoxicity through impaired autophagic flux. Therefore, these results strongly suggest that therapies aimed to restore the autophagic flux might prevent or attenuate the progression of NAFLD.

Keyword : Ephedrine, Mitophagy, Parkin, Mitochondrial oxidative stress, Hepatotoxicity, Sphingolipids, Dihydroceramide, Liver fibrosis

Student Number : 2012-21547

TABLE OF CONTENTS

CHAPTER I

Ephedrine-induced Mitophagy via Oxidative Stress in Human Hepatic Stellate Cells

CHAPTER II

Dihydroceramide is a Key Metabolite that Regulates Autophagy and Promotes Fibrosis in Hepatic Steatosis Model

LIST OF ABBREVIATIONS

ROS	Reactive oxygen species
ATP	Adenosine triphosphate
PINK1	Phosphatase and tensin homolog-induced putative kinase 1
TEM	Transmission electron microscopy
mtDNA	Mitochondrial DNA
nDNA	Nuclear DNA
FFA	Free fatty acids
LD	Lipid droplet
FBS	Fetal bovine serum
BCA	bicinchoninic acid
SOD2	Superoxide Dismutase 2
LC3	Light chain 3
PBS	Phosphate-buffered saline
SEM	Standard error of the mean
MMP	Mitochondrial membrane potential
rER	Rough endoplasmic reticulum
COXIV	Cytochrome c oxidase subunit 4

ptf-LC3	Tandem RFP-GFP–tagged LC3
siSCR	Scramble cells
NAFLD	Non-alcoholic fatty liver disease
NAS	Non-alcoholic steatosis
NASH	Non-alcoholic steatohepatitis
S1P	Sphingosine-1-phosphate
p62	Sequestosome 1, ubiquitin-binding protein p62
LSM710	Confocal laser scanning microscopy
SM	Sphingomyelin
Cer	Ceramide
dCer	Dihydroceramide
So	Sphingosine
Sa	Sphinganine
TG	Triacylglycerol
IS	Internal standard
CNs	Carbon numbers
DBs	Double bonds
Lamp1	Lysosomal-associated membrane protein 1

Lamp2	Lysosome-associated membrane protein 2
DIC	Dfferential interference contrast
α-SMA	α-smooth muscle actin
FGF-2	Basic fibroblast-growth factor
CCK-8	Cell Counting Kit
JC-1	Tetraethylbenzimidazolylcarbocyanine iodide
H_2DCFDA	2',7'-dichlorodihydrofluorescein diacetate
HSCs	Hepatic stellate cells
AST	Aspartate aminotransferase
ALT	Alanine aminotransferase
BMI	Body mass index
HA	Hyaluronic acid
GGT	γ-glutamyltransferase
PIIINP	Procollagen III amino-terminal peptide
TIMP1	Tissue inhibitor of matrix metalloproteinase 1
ELF	Enhanced liver fibrosis
FIB-4	fibrosis-4
PT	Prothrombin

FDA	Food and Drug Administration
WAT	White adipose tissue
BAT	Brown adipose tissue
CK18	cytokeratin 18
AMPK	AMP-activated protein kinase
HFD	High-fat diet
mTOR	Mammalian target of rapamycin
3-MA	3-methyladenine

LIST OF FIGURES

LITERATURE REVIEW

CHAPTER I

CHAPTER II

LIST OF TABLES

LITERATURE REVIEW

A. Current Management and Treatment of Nonalcoholic Fatty Liver Disease

Liver is the major organ that regulates whole body metabolism (Wang et al., 2018). Nonalcoholic fatty liver disease (NAFLD) represents a spectrum of liver disorder from fatty liver, characterized by hepatic fat deposition without inflammation, to non-alcoholic steatohepatitis (NASH), characterized by hepatic fat accumulation with inflammation, accumulating fibrosis, and eventually liver cirrhosis. NASH-related cirrhosis is recently a main cause of chronic liver disease and is related with liver cancer (Ofosu et al., 2018). NAFLD is represented by its progression from simple steatosis to steatohepatitis, fibrosis, and cirrhosis (Figure 1) (Mao et al., 2016).

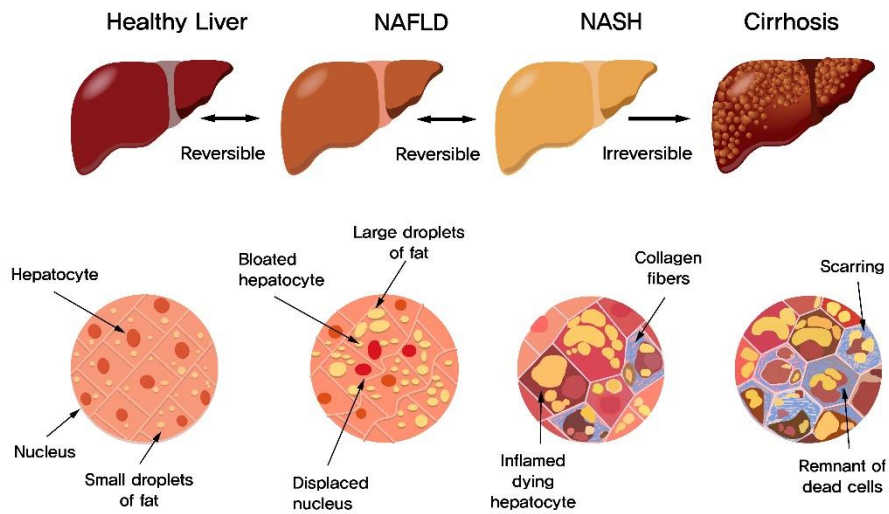

(http://www.hcv-trials.com/nash/NAFLD-NASH.asp)

Figure 1. NAFLD: progression of liver disease

Several studies have showed way at the management of fatty liver disease. However, there is no effective methods on the optimal management of NAFLD. According to Food and Drug Association (FDA), there are no drug therapies approved for the current treatment of NAFLD. This study aims to review current trends on NAFLD, with emphasis on identifying gaps in its diagnosis and management, and suggests future directions to overcome these limitations.

A summary of biomarkers or current clinical aids used to evaluate fibrosis can be seen in Table 1. Theses assessment shows convenient and non-invasive test, but the reliability and accuracy of the results is low. Also, the results are hard to interpret.

Table 1. Biomarkers for detection progressive liver fibrosis

Test	Panel components	Sensitivity (%)	Specificity (%)	Fibrosis stage
AST/ALT ratio	AST, ALT	21	90	F3-F4
AST/platelet ratio	AST, Platelet	30	93	F2-F4
BAAT score	BMI, Age, ALT, Serum Triglycerides	71	80	F3-F4
BARD	BMI, AST/ALT, Diabetes	87	33	F3-F4
ELF test	Age, HA, TIMP-1, PIIINP	80	90	F2-F4
Fibrometer	Platelet, G2 Macroglobulin, AST, Age, PT, HA, BUN	81	84	F2-F4
Fibrotest	α-2 Macroglobulin, Haptoglobin, GGT, Total Bilirubin, Apolipoprotein	15-77	77-90	F2-F4
FIB-4 score	Age, AST, Platelet Count, ALT	26-74	71-98	F3-F4
Hepascore	Age, Sex, Bilirubin, GGT, HA, α-2 Macroglobulin	76-87	84-89	F3-F4
NAFLD fibrosis score	Age, Hyperglycemia, BMI, Platelet, Albumin, AST/ALT	51	96	F3-F4

(Ofosu et al., 2018)

Liver biopsy remains the important standard for proving the diagnosis of NASH and estimation liver disease. However, liver biopsy is limited by its invasiveness, sampling error and cost. An accurate noninvasive methods for distinguishing NAFL from NASH with fibrosis are essential requirement for NAFLD patients' management. Several studies are under way to overcome these limitations. Other diagnostic methods show meaningful results in the use of hepatic collagen fractional synthesis rate (FSR), and plasma FSR, which correlates with hepatic fibrosis in humans. However, more studies are required to validate these findings.

Because of the increasing incidence of NAFLD, a large amount of effort is required to detect NAFLD in the early stage and reduce its progression. As mentioned previously, there are no current FDA-approved drugs for treatment NASH. However, for some patients, a number of therapeutic options to alleviate disease are available, as listed in Table 2.

Table 2. Therapeutic options in NASH

Drug	**Mechanism of action**
Orlistat	Oral inhibitor of gastric and pancreatic lipases
Metformin	Oral antihyperglycemic
Thiazolidinediones	Nuclear peroxisome proliferator-activated receptor-γ agonist
Liraglutide	Glucagon-like peptide-1 analog
Sitagliptin	Dipeptidyl peptidase 4 inhibitor

Statin	B-Hydroxy β-methylglutaryl-CoA reductase inhibitor
Ezetimibe	Cholesterol-absorption inhibitor
Ursodeoxycholic acid	Bile acid
Vitamin E	Antioxidant
Obeticholic acid*	Farnesoid X receptor agonist
Elafibranor*	Peroxisome proliferator-activated receptor α/δ agonist

*Ongoing clinical trials

(Ofosu et al., 2018)

Current numberless research has led to the development of novel therapies in NAFLD. However, it takes long follow-up period more than 15 years. NAFLD-related cirrhosis is a slow, progressive disease that takes years to develop medicine. Therefore, this clinical trial would be costly and challenging. NAFLD is emerging as the common cause of chronic liver disease in the worldwide and presents social and economic burden. If it is not resolved, a significant part of healthcare expense and resources will be required to cater for NAFLD related illness, increasing further healthcare cost (Ofosu et al., 2018). It is important to develop treatment by understanding the specific mechanisms of NAFLD.

B. Autophagy in Nonalcoholic Fatty Liver Disease

Autophagy is a highly-conserved lysosomal degradation mechanism, which plays an essential role in maintaining cellular integrity by eliminating protein aggregates and damaged or excessive organelles in mammalian cells (Wang et al., 2018). Autophagy selectivity depends on the type of stress, for example, mitochondrial stress promotes autophagy of damaged mitochondria (mitophagy), whereas lipid overload facilitates autophagy of lipid droplets (lipophagy). However, excessive and impaired autophagy triggers cell death (Zhang et al., 2018).

In the liver, autophagy suppresses protein aggregation, oxidative stress, lipid accumulation, inflammation, and chronic cell death (Wang, 2015). Moreover, autophagy has been implicated in the direct catabolism of fatty acids through lipophagy and inhibition of autophagy leads to the development of fatty liver and insulin resistance (Sinha and Yen, 2016). Lipophagy is involved in the reduction of lipid droplets observed during the activation of hepatic stellate cells (HSCs) during the onset of liver fibrosis (Codogno and Meijer, 2013).

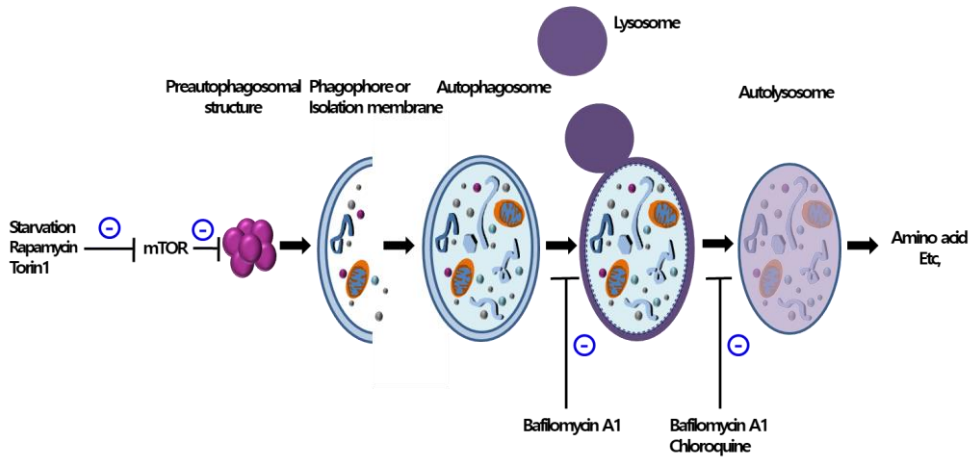

(Modified from Mizushima et al., 2010)

Figure 2. The Process of Macroautophagy

The process of autophagy in the liver can be seen in Figure 2. Hepatocyte triglyceride content was significantly increased when challenged with fatty acid supplement or cultured in methionine and choline-deficient medium with exogenous lipid supplement treated with 3-MA, a pharmacological inhibitor of autophagy (Mizushima et al., 2010). On the other hand, treatment with rapamycin, a pharmacological stimulator of autophagy through mTOR inhibition, significantly decreases lipid droplets (Lee et al., 2017). Recent studies showed that thyroid hormones, known to be important in promoting metabolism, probably stimulate fatty acid oxidation by induction of hepatic autophagy, which could be blocked by Atg5 siRNA (Sinha and Yen, 2016). Another study showed that treatment with caffeine reduces cellular lipids accumulation and the serum level of β-hydroxybutyrate, a product of lipolysis, and is accompanied with the increase of LC3-II (Zheng et al.,

2015). However, Atg5 knockdown in hepatocytes significantly increased hepatic lipids and reduced β-hydroxybutyrate levels (Lin et al., 2013). Another study indicated that pharmacological intervention with rapamycin (mTOR-independent inducer of autophagy) in high-fat diet (HFD)-fed mice clearly reduced hepatic triglyceride in blood, blood glucose and plasma insulin levels, indicating that modulation of autophagy alleviates NAFLD via an mammalian target of rapamycin (mTOR)-dependent or -independent pathway. Autophagy removes lipid droplets not only in NAFLD but also in other factor-induced fatty liver diseases such as ethanol-induced steatosis (Mao et al., 2016).

Hepatic fibrosis is the progressive accumulation of extracellular matrix that occurs in various chronic liver diseases, including NAFLD. HSCs function well in hepatic fibrosis, which may be a possible link with autophagy. HSCs activation is critical in liver fibrosis, as it leads to the production of excessive extracellular matrix. Recent study show that if autophagy could be selectively inhibited in HSCs and other fibrotic cells, a novel inhibitor for autophagy would be an attractive candidate for fibrosis treatment (Lee et al., 2017).

C. Effect of Mitophagy via Oxidative Stress in Nonalcoholic Fatty Liver Disease

Oxidative stress plays a central role in hepatocyte injury and disease progression from simple steatosis to NASH, but specific molecular species have not yet been identified (Alkhouri and McCullough, 2012). ROS are physiological by products of energy production from glucose breakdown and FFA β-oxidation and are more or less successfully controlled by endogenous radical scavenger system. However, in the NAFLD state there is an increase of FFA delivery to the hepatocytes and loss of suppression of FFA oxidation by insulin, generating levels of ROS that are beyond control of endogenous antioxidants (Lorbek and Rozm, 2012).

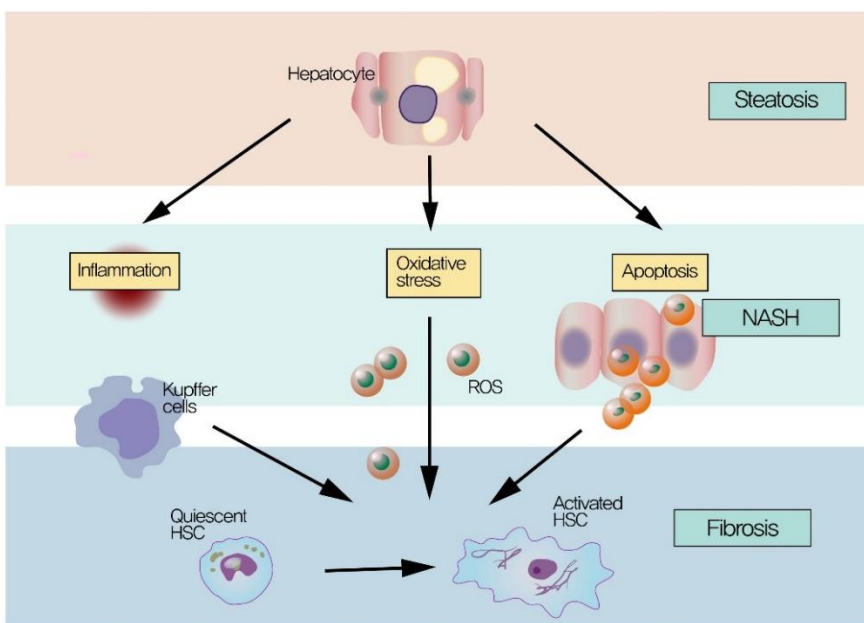

(Alkhouri and McCullough 2012)

Figure 3. Mechanistic pathways leading to disease progression from simple steatosis to NASH and advanced fibrosis

Mitochondria are an essential source of ATP for cellular function, but when damaged, mitochondria generate a plethora of stress signals, which lead to cellular dysfunction and eventually programmed cell death (Lee et al., 2017). Thus, a major component of maintaining cellular homeostasis is the recognition and removal of dysfunctional mitochondria through autophagy-mediated degradation, mitophagy (Hamacher-Brady and Brady, 2015). The mitophagy can reduce mitochondria-derived ROS formation and the release of pro-cell death factors from mitochondria.

Mitochondria may directly donate their membrane to form autophagosomes during Parkin-associated mitophagy. Thus there is a possibility of Parkin mediated autolipophagosome formation in hepatocytes by providing the autolipophagosomal membrane and subsequent reduction of steatosis by lipophagy (Eid et al., 2015). As shown Figure 4, mitophagy has been shown to require Parkin in *in vitro* models. Parkin is an evolutionarily conserved E3 ligase that is recruited to damaged mitochondria by phosphatase and tensin homolog-induced putative kinase 1 (PINK1) to initiate ubiquitination of mitochondrial outer membrane proteins and subsequent mitochondrial degradation via mitophagy (Williams et al., 2015). Thus, Parkin serve as therapeutic targets through damaged mitochondria in NAFLD progression.

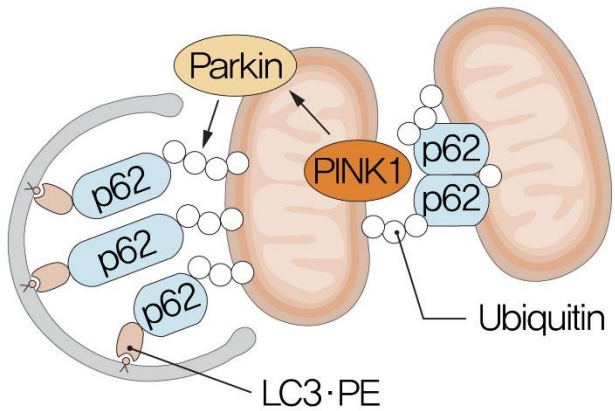

(Modified from Evans et al., 2017)

Figure 4. Model of key molecular events that mediate mitophagy

In response to mitochondrial damage, PINK1 activates the E3ubiquitin ligase Parkin, which targets many mitochondrial proteins. Selective autophagy receptors for mitophagy include p62. p62 proteins in the mitochondrial outer membrane directly mediate mitophagy by binding to LC3. Polyubiquitin/p62 oligomers cluster damaged mitochondria to favor mitophagy.

D. Autophagic Flux and Liver Metabolism

Many research has suggested a role for suppressed autophagy in the NAFLD. Defects in macrophage autophagy promoted hepatic inflammation and pro-inflammatory M1 macrophage polarization and decreased anti-inflammatory M2 macrophage polarization, leading to the initiation of liver injury in mice. Moreover, chronic HFD intake in mice interrupted the formation of autolysosomes in the liver. In addition to steatosis, mice with genetically predisposed or HFD-induced obesity exhibited suppressed autophagy shown as decreased autophagosome formation, lysosomal fusion or lysosome-associated membrane glycoprotein 2 (LAMP2) expression (Zhang et al., 2018).

In NAFLD, impairment in hepatocyte autophagy may not only promote steatosis but also might lead to NASH owing to the loss of autophagy's protective function against cell death. The moderate level of lipid droplets stimulates autophagy as a cell survival mechanism, but high concentrations block the autophagic flux and result in autophagic stress and cell damage (Wang, 2015).

Many studies represent similar results that intracellular reduction in lipid droplets was associated with an autophagy, suggesting that autophagy plays essential roles in lipolysis, called lipophagy, which may provide a new method to remove fat in addition to lipase-mediated lipolysis (Mao et al., 2016). Autophagy might stimulate lipid metabolism, and thus has therapeutic potential in NAFLD.

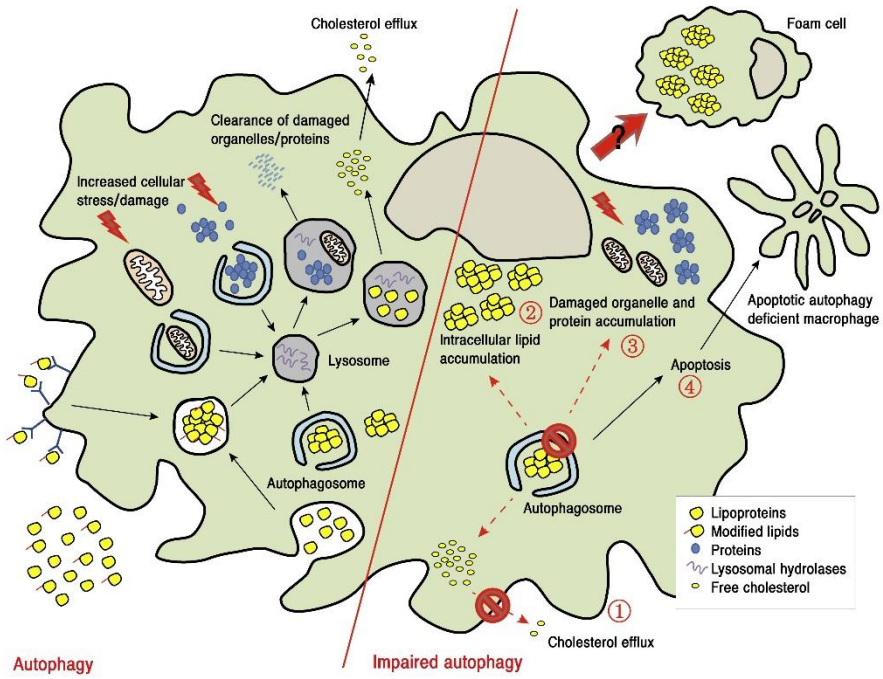

(Modified from Sergin and Razani, 2014)

Figure 5. Role of autophagy and impaired autophagy

CHAPTER I

Ephedrine-induced Mitophagy via Oxidative Stress in Human Hepatic Stellate Cells

1.1 Introduction

Usage of herbal dietary supplements has increased worldwide over the past several years. Among a plethora of herbal and dietary supplements, weight loss supplements are the most common type of supplement related to liver toxicity. In 2009, a warning was issued by the FDA after 23 cases of severe liver injury were attributed to weight loss formulations (Zheng and Navarro, 2015). Some studies refer and updates the most recent findings concerning the mechanisms through which different dietary compounds from natural products affect mitochondria functionality in healthy and pathological *in vitro* and *in vivo* models, focused on the pathways involved in mitochondrial biogenesis and apoptosis (Forbes-Hernández TY et al., 2006).

Standardized extracts of natural sources are commonly included in dietary supplements (Schmitt et al., 2012). The herb *Ephedra sinica* (also known as Chinese ephedra or Ma Huang), used in traditional Chinese medicine, contains alkaloids identical to ephedrine and pseudoephedrine as its principal active constituents (Chen and Schmidt, 1926). Ephedrine is the main substance in weight-loss formulations and has been widely used since the 1990s (Liu et al., 2013). Dietary supplements were restricted under the 1994 Dietary Supplement and Health Education Act (DSHEA), which did not require the submission of safety data for dietary supplement to the U.S. Food and Drug Administration (U.S. Food and Drug Administration,

1995). However, the U.S. Food and Drug Administration banned the sale of ephedra-containing supplements in 2004 due to accumulated cardiotoxicity data (U.S. Food and Drug Administration, 2004). In 2005, U.S. courts concluded (U.S. Federal District Court, 2005) that analysis for the dose-specific adverse effects of ephedrine-containing products is necessary (Dunnick et al., 2007). Many clinical cases have shown that ephedrine has potential hepatotoxicity (Reuben et al., 2010; Zhu et al., 2015). However, the signaling pathway for ephedrine-induced hepatotoxicity remains to be elucidated.

Mitochondria are essential organelles for cellular ATP. Damaged mitochondria generate stress signals, which eventually lead to programmed cell death. Autophagy-mediated degradation of damaged mitochondria is an important component for maintaining cellular homeostasis (Hamacher-Brady and Brady, 2015). Mitophagy is important for maintaining mitochondrial homeostasis by removing dysfunctional mitochondria (Williams and Ding, 2015). Parkin is an evolutionarily conserved E3 ubiquitin ligase that is essential for mitochondrial degradation by mitophagy. Phosphatase and tensin homolog-induced putative kinase 1 (PINK1) recruits Parkin to damaged mitochondria to initiate the ubiquitination of mitochondria (Williams et al., 2015). The PINK1-Parkin-activated mitophagy pathway may be a beneficial therapeutic target to ameliorate the progression of liver injury through removing damaged mitochondria (Williams and Ding, 2015). With Parkin downregulation, reduced mitophagy results in an increase of steatosis and the suppression of mitochondrial biogenesis (Eid et al., 2015).

Ephedrine has many adverse effects, therefore, it is important to explore the mechanism in liver toxicity. In this study, we studied the effect of ephedrine including ROS production and mitochondrial membrane potential changes in the LX-2 hepatic stellate cell line. Moreover, we tried to investigate the mechanism of ephedrine-induced liver toxicity, especially related to Parkin-mediated mitophagy.

1.2 Materials and Methods

1.2.1 Cell culture and treatment

The human hepatic stellate cell line LX-2 was kindly provided by Dr. HJ Rhee (Yonsei University, Seoul, Korea) and maintained in DMEM Glutamax without sodium pyruvate (Life Technologies, Grand Island, NY, USA). Culture media contained 10% fetal bovine serum (FBS, Hyclone), 1% penicillin/streptomycin (Hyclone). Cells were maintained at 37 ℃ in a humidified incubator with 5% CO_2. Ephedrine was purchased from Sigma-Aldrich (St Louis, MO, USA). The ROS scavengers, mitoTEMPO (2.5μM) were co-treated with ephedrine for 48 h.

1.2.2 Cell Viability assay

Cell viability was measured using Cell Counting Kit (CCK-8, Dojindo Molecular Technologies, Kumamoto, Japan). LX-2 cells were seeded in 96-well plates at 1×10^4 cells/well. Cell media were removed and treated with serial dilutions of ephedrine and incubated for 24 h, 48h, and 72h. Then, the cell media were removed, 10 μl CCK-8 solution was added, and the cells were incubated for another 1 h. The absorbance was measured with an ELISA microplate reader (Bio-Rad, Richimond, CA, USA) at 450 nm. Cell viability was calculated as follows: % cell viability = (absorbance of treated cells/absorbance average of untreated cells; control cells) × 100

1.2.3 Measurement of ATP production

To examine the energy metabolism of cells, ATP level was analyzed using the CellTiter-Glo luminescent cell viability assay kit (Promega, Madison, WI, USA). The cells were seeded on the white-walled 96-well optical bottom plate at 1×10^4 cells/well and incubated for 24 h. Then, serial dilutions of ephedrine were added, followed by incubation for another 24 h, 48h, 72h. All the wells were treated with 50 μl of CellTiter-Glo reagent for 1 min in a shaking incubator at 60 rpm with protective lights. The luminescence was measured by luminometer (Berthold, Bad Wildbad, Germany).

1.2.4 Measurement of reactive oxygen species

Reactive oxygen species were measured using 2',7'-dichlorodihydrofluorescein diacetate (H_2DCFDA, Life Technologies) and fluorescence intensity was measured using the Incucyte HD imaging system (Essen Bioscience, Ann Arbor, MI, USA). The Incucyte HD imaging system was used to measure the intensity of H_2DCFDA fluorescence in each captured image at different times. We evaluated the changes in reactive oxygen species (ROS) by ephedrine at different times. After treatment with ephedrine and 5μM H_2DCFDA, fluorescence intensity was measured every 30min.

1.2.5 Protein expression analysis

The cell pellet was lysed in an EzRipa buffer (ATTO, Tokyo, Japan). Lysates were collected by centrifugation at 13,000 rpm for 20 min. Protein concentration was measured using the bicinchoninic acid (BCA) method (Pierce, Waltham, MA, USA). Equal amounts of protein were separated on SDS-PAGE gels and transferred to membranes using an iBlot system (Life Technologies). Membranes were blocked with 5% skim milk in TTBS at room temperature for 1h. They were immunoblotted with specific primary antibodies Superoxide Dismutase 2 (SOD2, 1:500) and Actin-HRP (1:2000) (Santa Cruz Biotechnology, Santa Cruz, CA, USA). Light chain 3 (LC3, 1:1000) antibody was purchased from Cell Signaling (Danvers, MA, USA). PINK1 (1:2000), Parkin (1:2000), and p62/SQSTM1 (1:10000) antibodies were purchased from Abcam (Cambridge, MA, USA). Blots were performed with the corresponding anti-rabbit, anti-goat, or anti-mouse IgGs conjugated with horseradish peroxidase (AbFrontier, Seoul, Korea) and detected using the ECL reagent (EMD Millipore, Darmstadt, Germany).

1.2.6 Mitochondrial membrane potential

Mitochondrial membrane potential was measured using 5′,6,6′-tetrachloro-1,1′,3,3′-tetraethylbenzimidazolylcarbocyanine iodide (JC-1, Life Technologies). After 24h of ephedrine treatment, 2μg/ml JC-1 dye was added to the cells at 37 °C for 30min. The cells were washed with PBS three times. Mitochondria images were

obtained by confocal laser scanning microscopy (LSM710, Carl Zeiss Microscopy GmbH, Oberkochen, Germany) and FACS AriaII flow cytometer (BD, Franklin Lakes, NJ, USA). Fluorescence was measured at 514 nm for excitation and at 529 nm for emission. Data was analyzed using Flow Jo software (FLOWJO., LLC, San Carlos, CA, USA)

1.2.7 Mitochondria staining

Staining of mitochondria was performed using MitoTracker Red CMXRos and MitoTracker® Deep Red FM (Life Technologies). Treatment of cells with 100nM MitoTracker was performed for 15min at 37 °C and the cells were washed with PBS three times. Mitochondria images were obtained with LSM710. Red fluorescence was measured at 579 nm for excitation and at 599 nm for emission. Deep red fluorescence was measured at 644 nm for excitation and at 665 nm for emission.

1.2.8 Immunofluorescence

Cells were seeded onto 2 well chamber slides at 7×10^3 cells/well and incubated overnight. After 24 h of incubation, slides were blocked with 3 % BSA in Phosphate-buffered saline (PBS) and incubated overnight at 4 °C with primary antibody against Parkin (1:200, Abcam, Cambridge, MA, USA). After washing three times with TTBS, the slides were incubated with a secondary antibody with

fluorescence such as Alexa Fluor 488 (Life Technologies) for 1 h at room temperature. After washing three times with PBS, images were obtained with LSM710.

1.2.9 Transmission electron microscopy (TEM) analysis

Cells were incubated with the treatment of ephedrine. After washing with PBS, cells were immediately fixed with Karnovsky's solution. After fixation, cells were stained with 0.5% aqueous uranyl acetate for 20 min, dehydrated with graded ethanol solutions, and embedded in Spurr's resin. Thin sections were cut with an ultramicrotome and stained with 2% uranyl acetate and Reynolds's lead citrate. Sections were examined using a LIBRA 120 transmission electron microscope (Carl Zeiss) at an accelerating voltage of 80 kV.

1.2.10 Quantification of mitochondrial DNA copy number

Mitochondrial copy number was measured using real-time PCR as previously reported (Zhang et al., 2009). Real-time PCR primers were designed as follows:

mitochondrial DNA (mtDNA) 5'-ACCGCGGTCATACGATTAAC-3' (Forward), 'CCCAGTTTGGGTCTTAGCTG-3' (Reverse);

nuclear DNA (nDNA) 5'-CGCGGTTCTATTTTGTTGTTGGT-3' (Forward), 5'-AGTCGGCATCGTTTATGGTC-3' (Reverse).

1.2.11 ptf-LC3 assay

The ptf-LC3 construct was purchased from ADD GENE (Cambridge, MA, USA). Cells were transfected using the Neon transfection system (Life Technologies) and treated with ephedrine. After treatment, we counted the number of green and red puncta using Image J software. Autophagic puncta was obtained with LSM710.

1.2.12 Parkin silence cell

The Parkin siRNAs were purchased from Bioneer (Daejeon, Korea). For the generation of a Parkin-downregulated cell, cells were cultured in T-75 flask (Corning Incorporated, Corning, NY, USA). After cell stabilization, siRNAs were transfected using Neon® transfection system (Life Technologies). We performed 3 different siRNA sequence (#1: UGAGGAAUGCUGGACGU, #2: GACAAGGUGUUUCUCUGUA, #3: CUGGUUUUCCAGUGCAACU).

1.2.13 Statistical analysis

All data were presented as mean ± standard error of the mean (SEM). Puncta number cells were statistically compared using Two-way ANOVA with graph pad prism5 software (La Jolla, CA, USA). Statistical significance was considered when the *P* value was less than 0.05.

1.3 Results

1.3.1 Effect of ephedrine on cell viability and ATP production

Based on the cell viability and ATP production, ephedrine concentration was calculated in 120 and 240μl/ml by IC_{50}. After treatment of ephedrine, ATP production is more severe cytotoxicity than cell viability (Figure 1.1A and 1.1B).

A

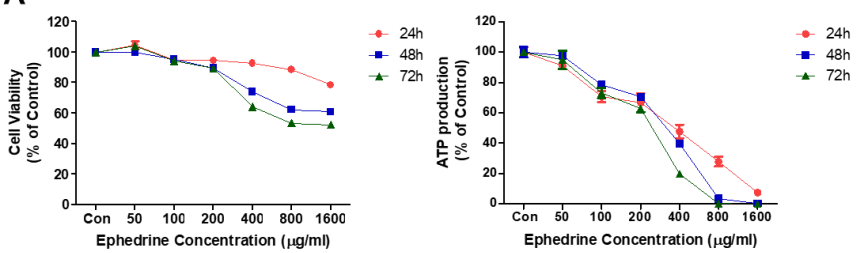

B

Ephedrine (μg/ml)	IC_{50} (R^2)			95% Confidence Intervals		
	24h	48h	72h	24h	48h	72h
CCK-8	547469 (0,8279)	4069 (0,9231)	1635 (0,8984)	2062 to 11536	793.2 to 1625	533.9 to 930.7
ATP	493.5 (0.9405)	405.6 (0.9687)	245.3 (0.9535)	285.1 to 854.3	289.0 to 569.2	163.2 to 368.9

Figure 1.1. Cell viability and ATP production in LX-2 cells

(A) LX-2 cells were treated with diverse concentrations of ephedrine (50 - 1600 μg/ml for 24 h, 48h, and 72h). Cell viability was measured by the CCK-8 assay. The reduction of ATP production by ephedrine was detected in LX-2 cells. (B) IC_{50} in cell viability and ATP production.

1.3.2 Ephedrine induces ROS production

ROS production was measured according to H_2DCFDA fluorescent intensity with live imaging. The results showed that ephedrine increased ROS production, which reached the highest level after 6h of treatment (Figure 1.2A). Manganese superoxide dismutase 2 (SOD2) provides crucial mitochondrial antioxidant defense against superoxide production (Silva et al., 2005). SOD2 level was also increased after 6h treatment with ephedrine (Figure 1.2B).

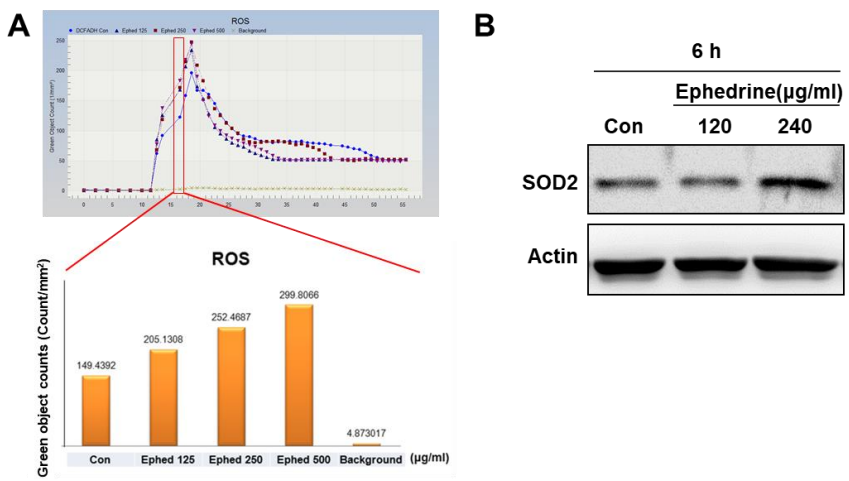

Figure 1.2. Ephedrine induces ROS production

(A) H_2DCFDA fluorescent intensity for measurement of ephedrine-induced ROS production at different times. After 6h of treatment with ephedrine, the highest level of ROS production was observed. (B) Expression of SOD2 protein level after 6h of treatment with ephedrine.

1.3.3 Ephedrine induces MMP loss

Loss of mitochondrial membrane potential (MMP) was detected via JC-1 staining to evaluate the mitochondrial damage. Cells with low MMP due to mitochondrial damage exhibited green fluorescence signals. After treatment with ephedrine, the decrease in the signal intensity of red fluorescence was compared to the control group Also, green fluorescence was increased after treatment of ephedrine (Figure 1.3A). Counts for green fluorescence objects were increased in ephedrine treated groups compared to the control group because of ephedrine-induced mitochondrial damage (Figure 1.3B). Histogram representing green fluorescence level relative to the control. (Figure 1.3C).

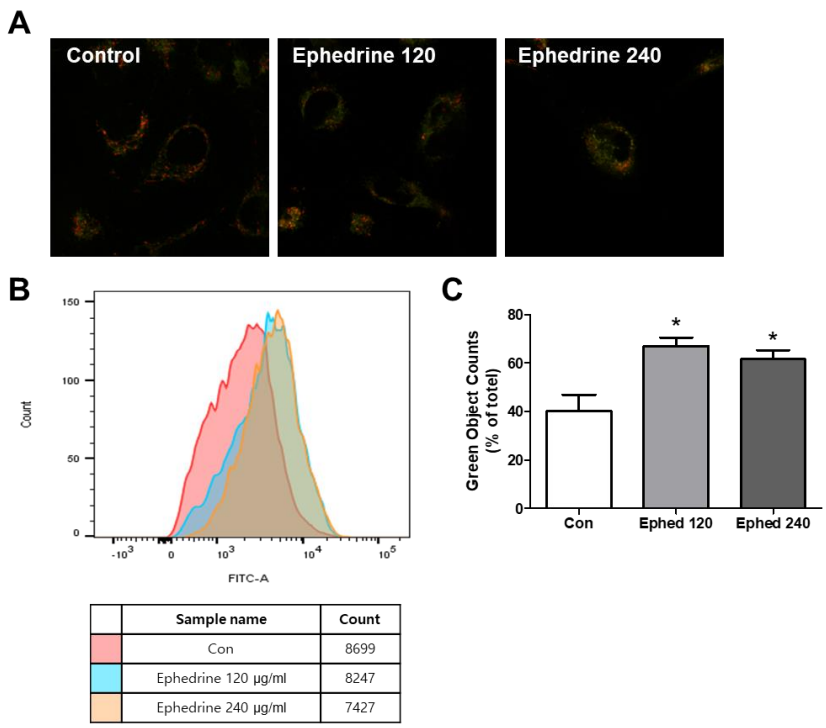

Figure 1.3. Ephedrine induces depolarization in LX-2 cells

(A) Alteration of mitochondrial membrane potential (MMP) was evaluated with JC-1 staining. (B) Flow cytometric analysis of green object counts (% of total) after treatment with ephedrine. Green fluorescent cells increased after treatment with ephedrine. (C) Histogram representing green fluorescence level relative to the control.

1.3.4 Cellular morphological change by ephedrine exposure

Ephedrine-induced changes of cellular morphology were examined by TEM analysis. Ephedrine-induced damage in mitochondrial morphology in a time-dependent manner. Rough endoplasmic reticulum (rER), encapsulating damaged mitochondria, and mitochondrial swelling were observed in TEM images. After 72h of treatment, autolysosomes were observed in ephedrine-treated cells (Figure 1.4).

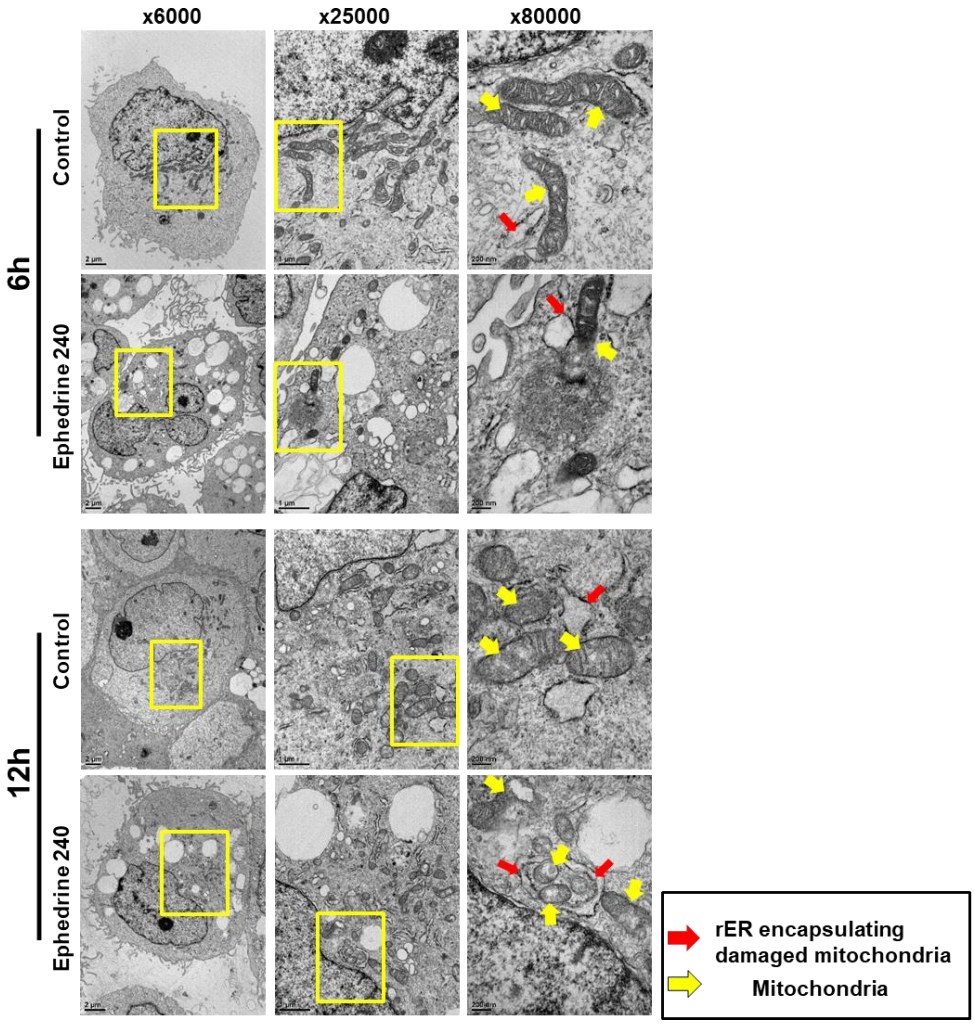
x6000
x25000
x80000
6h
Control
Ephedrine 240
12h
Control
Ephedrine 240
rER encapsulating damaged mitochondria
Mitochondria

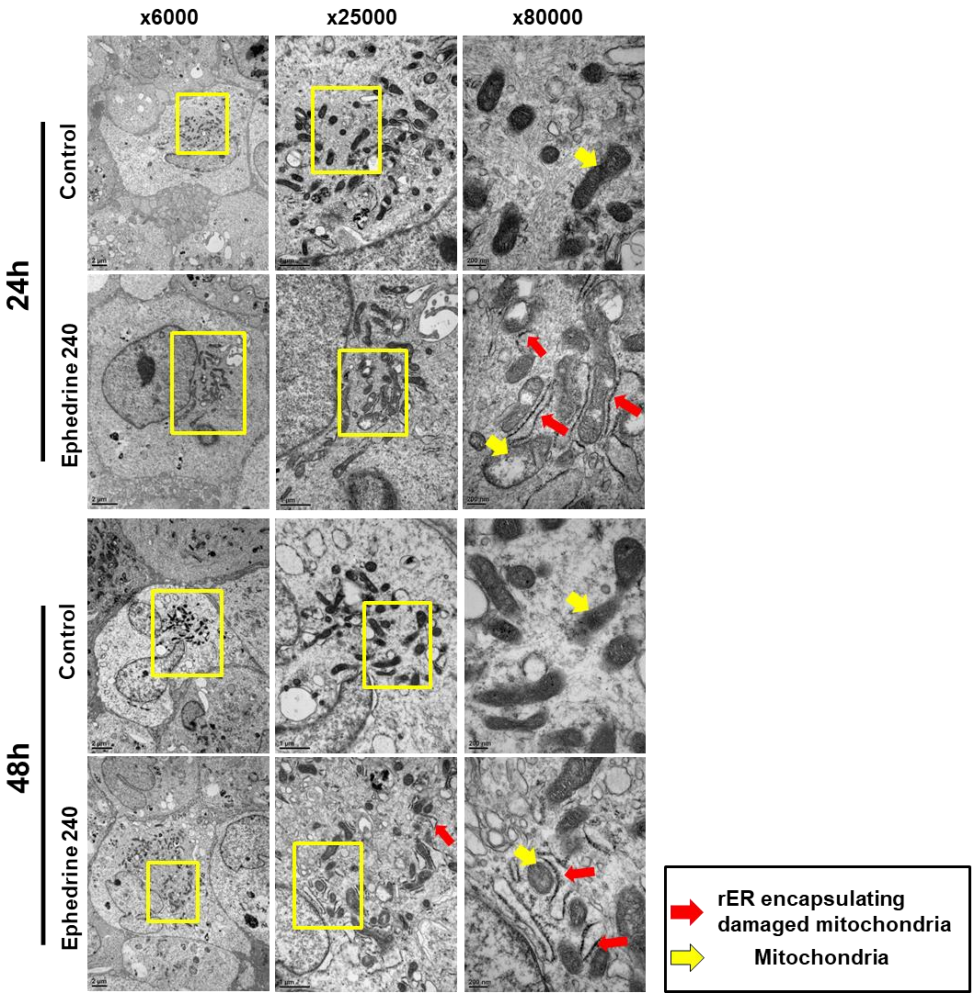
x6000
x25000
x80000
24h
Control
Ephedrine 240
48h
Control
Ephedrine 240
rER encapsulating damaged mitochondria
Mitochondria

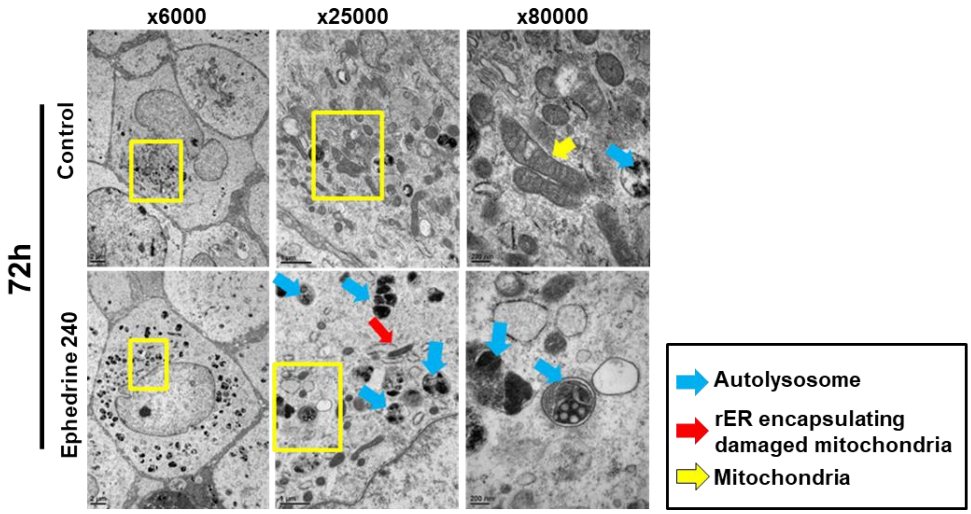

Figure 1.4. Cellular morphological change by ephedrine exposure

Analysis of cellular morphology change after treatment with ephedrine at different times using transmission electron microscope (TEM). Rough endoplasmic reticulum (rER) encapsulating damaged mitochondria were observed in the early stage. After 72h of treatment, autolysosomes increased in ephedrine-treated cells. (Scale bars: 2, 1, and 0.2 μm.)

1.3.5 Mitochondrial damage reduced the copy number of mitochondrial DNA

Moreover, mitochondrial DNA (mtDNA) content was reduced in the ephedrine-treated group by about 40% compared with the control group. The ratio of mtDNA/nuclear DNA (nDNA) was also decreased in ephedrine-treated cells (Figure 1.5A). Furthermore, cytochrome c oxidase subunit 4 (COX IV) was

decreased after treatment with ephedrine in a dose-dependent manner (Figure 1.5B).

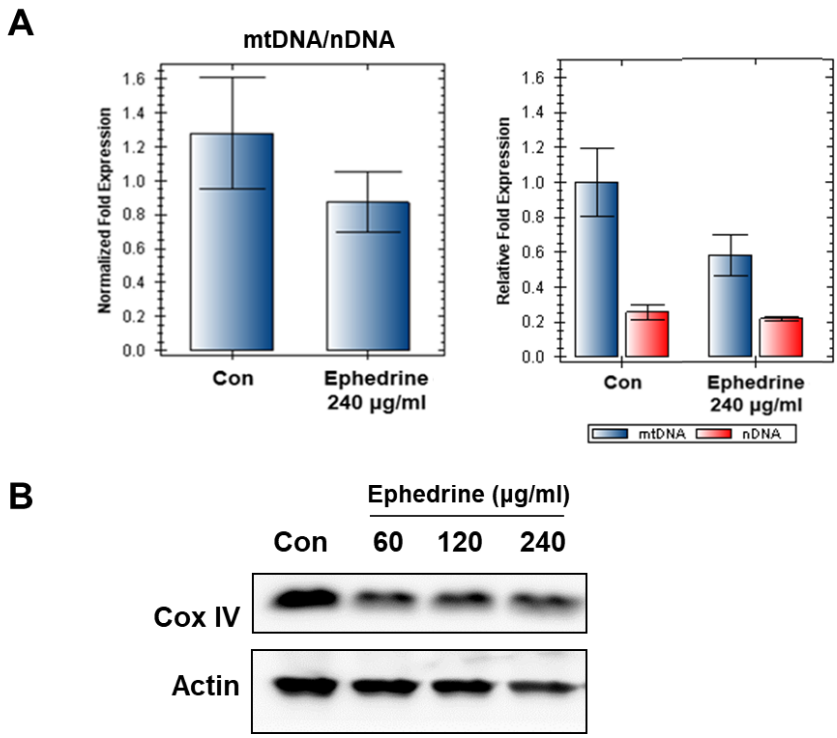

Figure 1.5. Mitochondrial damage reduces the copy number of mitochondrial DNA (mtDNA)

(A) The ratio of mtDNA/nuclear DNA (nDNA) decreased after treatment with ephedrine. The quantity of DNA also decreased. (B) Cox IV expression level was analyzed to evaluate mitochondrial copy number.

1.3.6 Ephedrine-induced mitophagy and high autophagic flux

Time course analysis for mitophagy-related protein levels was performed after treatment with ephedrine. After 48h of treatment of ephedrine, Parkin, PINK1, p62 and LC3 protein levels were higher than at other time-points (Figure 1.6A). Tandem RFP-GFP–tagged LC3 (ptf-LC3) was also examined for the classification of autophagic flux. A yellow signal indicates autophagosome, and a red signal indicates autolysosome. LC3 puncta was enhanced after treatment with ephedrine for 48h (Figure 1.6B). Moreover, after treatment with ephedrine for 48h, the red signals were significantly increased compared to the control group (Figure 1.6C). Ephedrine also increased Parkin expression in LX-2 cells confirmed by immunofluorescence (Figure 1.6D).

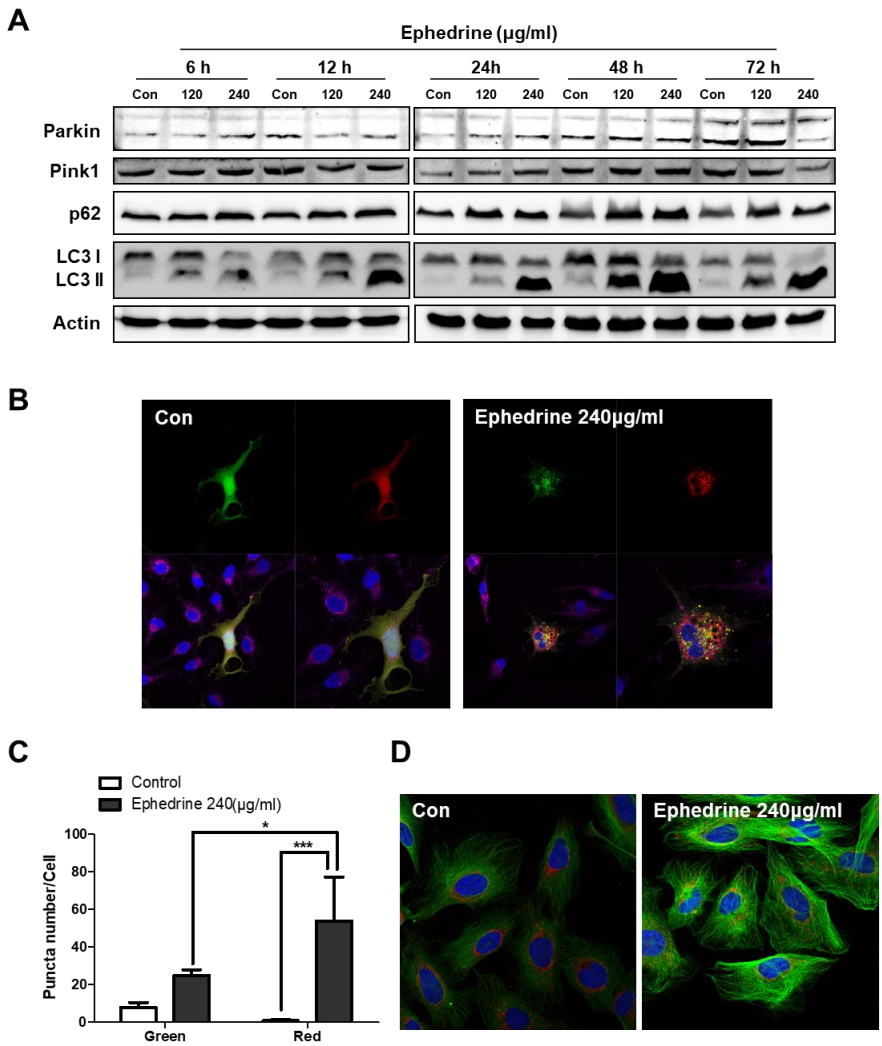

Figure 1.6. Ephedrine induces mitophagy and high autophagic flux

(A) Mitophagy-related protein levels were increased after treatment of ephedrine at different times. Protein expression showed the highest levels at 48h. (B) Autophagic flux using RFP-GFP–tagged LC3 (ptf-LC3) and mito-tracker (deep red). Ephedrine-treated cells showed high autophagic flux. (C) Counting of green and red puncta in control and ephedrine-treated cells. Puncta number was significantly increased in

ephedrine-treated cells. (D) Immunofluorescence was performed for Parkin (green), mito-tracker (red) and DAPI (blue). Expression of Parkin was significantly increased by 240 μg/ml of ephedrine treatment. Intensity of Mito-tracker was decreased after treatment with ephedrine. Data were expressed as mean ± SEM. *: significantly different from each group ($p < 0.05$). ***: significantly different from each group ($p < 0.001$).

1.3.7 Ephedrine induces Parkin-mediated mitophagy

Significant silencing of Parkin-downregulated cell was confirmed by Western Blot (Figure 1.7A). We evaluated mitochondrial morphology after treatment with ephedrine in Parkin-downregulated cells. After 12h treatment with ephedrine, siSCR cells showed vacuoles, however, the formation of the ephedrine-induced vacuole was inhibited in siParkin. After 72h treatment with ephedrine, the mitochondrial morphology of siSCR cells was not significantly different from only ephedrine treated cells. Autolysosomes and damaged mitochondria were also observed in siSCR cells. However, in siParkin cells, cellular status was recovered in siParkin cells. (Figure 1.7B). Downregulation of Parkin cells were reduced LC3 ratio (LC3-II/LC3-I). Also, Treatment of ephedrine in siParkin cells were decreased LC3 ratio compared to Scramble cells (siSCR) (Figure 1.7C).

1.3.8 Ephedrine induces mitophagy via oxidative stress

mitoTEMPO is mitochondrial ROS scavenger that act on the mitochondrial matrix. We evaluated increased expression of mitophagy-related protein with treatment of ephedrine. Further examination showed that mitoTEMPO ameliorated ephedrine-induced mitophagy (Figure 1.7D).

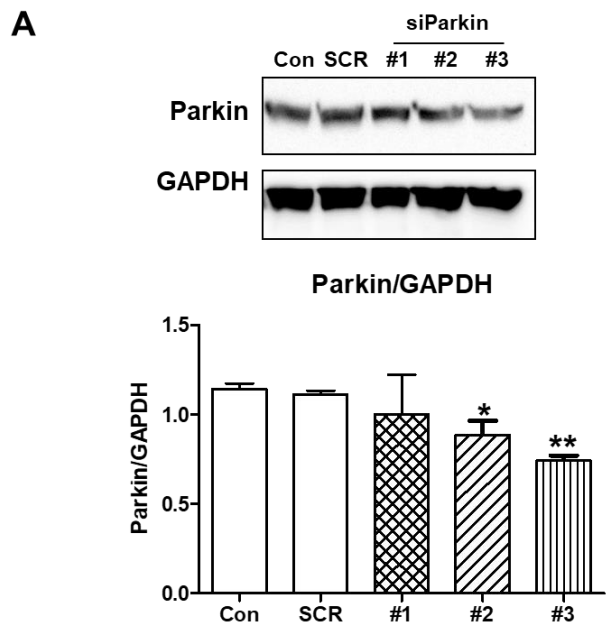

B

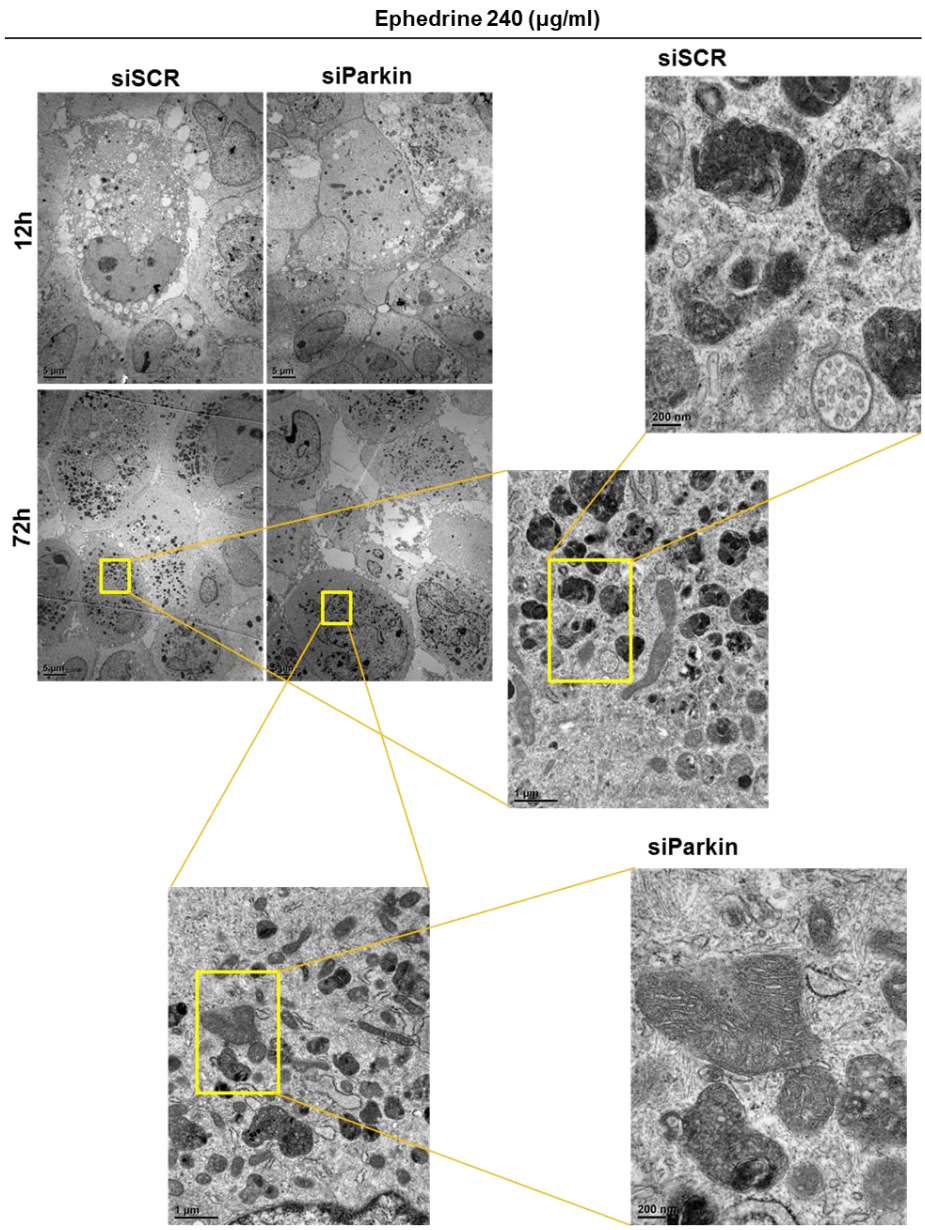
Ephedrine 240 (μg/ml)
siSCR
siParkin
12h
72h
5 μm
5 μm
5 μm
5 μm
siSCR
200 nm
1 μm
siParkin
1 μm
200 nm

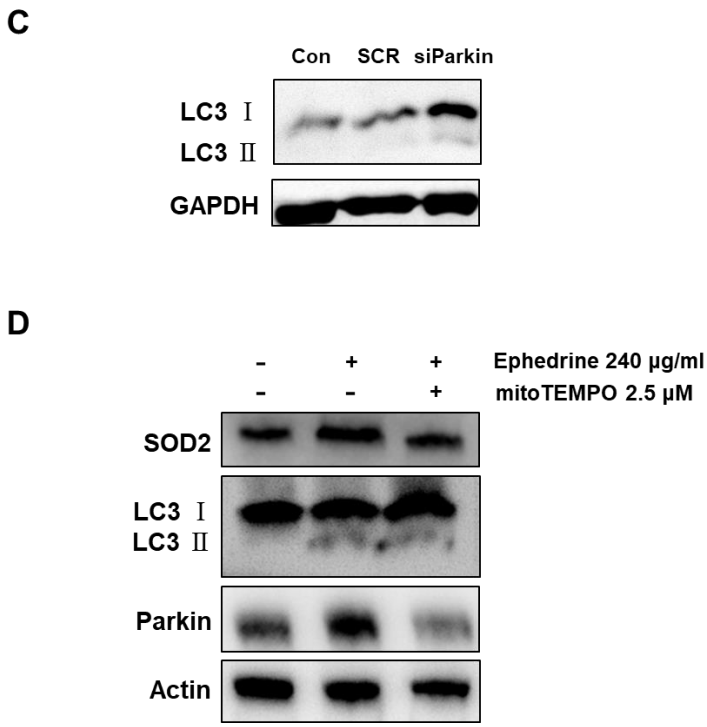

Figure 1.7. Ephedrine induces Parkin-mediated mitophagy

(A) Silencing of Parkin-downregulated stable cell line was confirmed by Western Blot. We performed 3 different siRNA sequence. As a result, we choose number 3 (#3) sequence. (B) Comparison of cellular morphology in ephedrine-treated siSCR and siParkin cells (12, 72h after ephedrine treatment). In ephedrine-treated siSCR group, vacuoles and autolysosomes were observed. In ephedrine-treated siParkin groups, mitophagic change was alleviated. Scale bars: 5, 1, and 0.2 μm. (C) siParkin cells were reduced LC3 ratio (LC3-II/LC3-I). (D) ROS-related protein and autophagy-related gene expression were alleviated by mitoTEMPO treatment.

*: significantly different from control ($p < 0.05$). **: significantly different from control ($p < 0.01$).

1.4 Discussion

Mitochondria play important roles in numerous cellular processes involved in cell life and death and the regulation of these processes is implicated in several metabolic, degenerative and hyperproliferative diseases (Forbes-Hernández TY et al., 2006). The rate of mitophagy is enhanced during physiological conditions of increased reactive oxygen species (ROS) production or when the MMP decreases (Hood et al., 2015). Increased ROS level and decreased MMP are common characteristics of mitophagy activation (Villanueva Paz et al., 2015). Early ROS production in cells leads to lysosomal destabilization, and autophagosome/lysosome fusion becomes strongly impaired (Radogna et al., 2015). In this study, we evaluated ephedrine-induce hepatotoxicity in the LX-2 hepatic stellate cell line. Our results showed that ephedrine increased intracellular ROS production. Moreover, ephedrine induced loss of MMP and affected the morphology of mitochondria.

Increased ROS generation leads to MMP defects, which induce the accumulation of PINK1 on the outer membrane of the damaged mitochondria. PINK1 accumulation on the mitochondrial membrane recruits Parkin to the dysfunctional mitochondria. Parkin then mediates the autophagic elimination of the damaged mitochondria (Murata et al., 2015; Pickrell and Youle, 2015). Our study indicates that ephedrine induces PINK1 and Parkin mediated mitophagy. During Parkin-associated mitophagy, mitochondria may donate their membranes to form

autophagosomes (Eid et al., 2015). In TEM analysis, ephedrine formed vacuoles and rER, encapsulating damaged mitochondria. Ephedrine is one of the substances that cause lysosomal vacuolation in cells (Ohkuma and Poole, 1981). However, our study demonstrates that these ephedrine-induced vacuoles were not derived from lysosomes. The formation of the vacuoles remain to be elucidated. After 48h of ephedrine treatment, we observed the vacuoles change into autolysosomes over time.

Reduced copy number for mitochondrial DNA is a biomarker of mitochondrial disorder (Liu et al., 2015; Pyle et al., 2015). Relative mtDNA content to nDNA decreases after treatment with ephedrine. Cox IV also decreases as a mitochondrial marker. The number of autophagosomes and autophsosomes were counted using tandem-labeled mCherry-EGFP-LC3 (ptf-LC3) vectors to measure autophagic flux (Gump and Thorburn, 2014). After fusion of the autophagosomes with lysosomes, the green signal disappears because of the lysosome pH (Gump et al., 2014). According to our data, ephedrine induced a decrease in mtDNA content with autolysosome increase.

Parkin regulates mitochondrial biogenesis and mitochondrial dynamics through fission and fusion, in addition to selective protein extraction from mitochondria via vesicle formation (Dorn, 2015). Parkin and PINK1 are required for Parkin-dependent mitophagy (Ivankovic et al., 2015). PINK1 is positioned on the mitochondrial outer membrane during mitochondrial depolarization, which activates Parkin's E3 ligase activity through the phosphorylation of Ser65 in Parkin's ubiquitin-like (UBL) domain (Williams and Ding, 2015a). Excessive mitophagy

may contribute to metabolic and bioenergetic collapse, and to eventual cell death (Kim and Choi, 2014; Shi et al., 2014). In addition to mitophagy, mitochondria can be eliminated by extrusion from the cell (mitoptosis) (Daniel J Klionsky et al., 2016). Our results show that ephedrine enhances the expressions of PINK1 and Parkin. Moreover, after treatment with ephedrine in siParkin cells, mitochondrial damage was recovered.

CHAPTER II

Dihydroceramide is a Key Metabolite that Regulates Autophagy and Promotes Fibrosis in Hepatic Steatosis Model

2.1 INTRODUCTION

Non-alcoholic fatty liver disease (NAFLD) is an increasingly common chronic liver disease worldwide. NAFLD includes fatty liver, non-alcoholic steatosis (NAS), and non-alcoholic steatohepatitis (NASH) with progressive fibrosis, cirrhosis, and hepatocellular carcinoma. Although oxidative stress and pro-inflammatory cytokines are associated with NASH pathogenesis, cellular mechanisms involved in liver-cell injury contributing to the progression from NAS to NASH remain unclear (Gonzalez-Rodriguez et al., 2014).

Hepatocytes are major cellular storages for neutral lipids in the form of triglycerides and cholesterol esters contained in specialized organelles termed lipid droplets (LD) (Martin and Parton, 2006; Thiele and Spandl, 2008). Recent studies have clearly demonstrated that autophagy can mediate hepatocellular lipid metabolism and that the breakdown of intracellular LD can be stored by the process of lipophagy (Singh et al., 2009). Autophagy is required to maintain liver homeostasis. In NAFLD, impairment in hepatic autophagy may not only promote steatosis, but also lead to NASH because of the loss of autophagy's protective function against cell death. Thus, alteration in autophagy is an underlying mechanism for several common hepatic diseases, including fatty liver (Czaja et al., 2013). Excessive uptake of free fatty acids (FFA) may overwhelm cellular capacity to store and utilize LD, eventually leading to hepatocellular steatosis (Schaffer, 2003; Feyza Gunduz, 2012). Therefore, FFA-induced hepatic stellate cell activation in

hepatocytes plays an important role in the pathogenesis of NAFLD (Malhi and Gores, 2008; Neuschwander-Tetri, 2010).

Sphingolipids are key regulators of cellular processes, including apoptosis, migration, cell growth, adhesion, and autophagy (Young et al., 2013). Sphingolipid-induced apoptosis and autophagy can address how sphingolipids mediate the "switch" between cell survival and cell death. Because of differential regulation of apoptosis and autophagy by sphingolipid metabolites, the sphingolipid network has emerged as a novel molecular switch between apoptosis and autophagic pathways (Young et al., 2013). Recent research on sphingolipids has focused on ceramide and sphingosine-1-phosphate (S1P) in autophagy. Not many studies have been focused on dihydroceramide. It has been suggested that dihydroceramide might be associated with autophagy (Signorelli et al., 2009; Bedia et al., 2011; Gagliostro et al., 2012; Young et al., 2013). However, the signaling pathway by which dihydroceramide exerts its pro-autophagic effect remains to be elucidated. In addition, no study has explained the role of dihydroceramide and autophagy in the FFA-induced steatosis model. Therefore, the objective of this study was to find out the relationship between dihydroceramide and autophagy in the progression of NAFLD.

In this study, we used an overload of FFA to human liver cells to represent a cellular model of steatosis mimicking benign chronic steatosis (Gomez-Lechon et al., 2007). These hepatic cellular models are suitable for experimental investigation of the impact of fat over accumulation in the liver, excluding other factors that could influence hepatocyte behavior. We demonstrated that the accumulation of

dihydroceramide was involved in the impairment of autophagic flux. FFA treatment affected liver fibrosis by not only DhCer upregulation but also Cer and other sphingolipids as well as TG content. FFA-induced dihydroceramide impaired autophagic flux and activated fibrogenic pathways. To address dihydroceramide autophagy regulation, we used inhibitors of key sphingolipid metabolism enzymes controlling the biosynthesis of dihydroceramide in order to find out the relationship of autophagy and dihydroceramide metabolism in FFA-induced hepatic stellate cell activation, but also investigated the mechanism that could increase the dihydroceramide level, a cause of hepatic steatosis in the human hepatic stellate LX-2 cells, which are the major cell type of fibrosis in injured liver. The contribution of hepatocyte-derived cell death signal to stellate cell activation is independent of inflammatory response, because the addition of hepatocyte apoptotic fragments has a direct fibrogenic effect in cultured stellate cells (Puche et al., 2013). Therefore, activated LX-2 cells are the most crucial factor involved in liver fibrosis (Giraudi et al., 2015). We presented the role of dihydroceramide in a cellular steatosis model and found that dihydroceramide could be a potential contributing factor to the progression of NAFLD.

2.2 Materials and Methods

2.2.1 Human liver-cell culture

Human liver Chang cells were purchased from ATCC (Manassas, VA, USA) and maintained in Dulbecco's modified Eagle's medium (DMEM, Hyclone, Pittsburgh, PA, USA). Human liver stellate cell line LX-2 was kindly provided by Dr. HJ Rhee (Yonsei University, Seoul, Korea) and maintained in DMEM Glutamax without sodium pyruvate (Life Technologies, Grand Island, NY, USA). Culture media contained 10% heat-inactivated fetal bovine serum (FBS, Hyclone), penicillin (100 IU/mL), and streptomycin (10 μg/mL) (Hyclone). Cells were maintained at 37 °C in a humidified incubator with 5% CO_2.

2.2.2 FFA preparation

FFA was conjugated with oleic acid and palmitic acid to achieve an appropriately 2:1 (oleic acid-to-palmitic acid) molar ratio. Oleic acid and palmitic acid were conjugated to bovine serum albumin as described previously (Park et al., 2014; Park et al., 2014). The final concentration of FFA was 5 mM. Stock solution was kept at -20 °C until use.

2.2.3 Inhibition of sphingolipid metabolism

Inhibitor XM462 was purchased from Fundacio Bosch i Gimpera (Barcelona, SPAIN) (Munoz-Olaya et al., 2008). The final concentration of XM462 in FFA co-treatment was 8 μM. Myriocin and fumonisin B1 were purchased from Sigma-Aldrich (St Louis, MO, USA). The concentration and treatment duration of myriocin and fumonisin B1 for cell study was 5 μM for 24 h.

2.2.4 Protein expression analysis

Cell pellets were lysed in an EzRipa buffer (ATTO, Tokyo, Japan). Lysates were collected by centrifugation at 13,000 rpm for 20 min. Protein concentration was measured using the bicinchonic acid (BCA) method (Pierce, Waltham, MA, USA). Equal amounts of protein were separated on SDS-PAGE gels and transferred to membranes using an iBlot system (Life Technologies). Membranes were blocked with 5% skim milk in TTBS at room temperature for 1 h. They were immuno-blotted with specific primary antibodies light chain 3 (LC3, Cell Signaling, Danvers, MA, USA) and p62 (Abcam, Cambridge, MA, USA). Blots were then incubated with corresponding anti-rabbit, anti-goat, or anti-mouse IgGs conjugated with horseradish peroxidase (AbFrontier, Seoul, Korea). Immuno-reactive proteins were detected using ECL reagent (EMD Millipore, Darmstadt, Germany).

2.2.5 Measurement of autophagosomes

Autophagosomes were measured with a CYTO-ID® Autophagy detection kit (Enzo Life Science, Farmingdale, NY, USA). Briefly, cells were incubated for 24 h after treatment followed by staining with 1X CY-ID solution for 3 h. Cell activity was detected using Multiple Plate Reader victor 3 (PerkinElmer, Waltham, MA, USA) and fluorescent imaging with confocal laser scanning microscopy (LSM710, Carl Zeiss Microscopy GmbH, Oberkochen, Germany). Fluorescence was determined at 480 nm for excitation and 530 nm for emission.

2.2.6 Lipid profiling sample preparation

HPLC-grade methanol, acetonitrile, water, and 2-propanol were purchased from J.T. Baker (Avantor Performance Material, Inc, PA, USA). HPLC-grade formic acid was purchased from Fluka Analytical and Sigma Aldrich Chemie GmbH (Steinheim, Germany). Chloroform and ammonium formate were purchased from Sigma-Aldrich (St. Louis, MO, USA). Lipid standards, SM (d18:1-12:0), Cer (d18:1-12:0), dCer (d18:1-12:0), So (d17:1), and Sa (d17:0) were purchased from Avanti Polar Lipids, Inc. TG (11:1-11:1-11:1) was purchased from Larodan Fine Chemicals AB (Malmö, Sweden).

Each lipid standard was dissolved in chloroform/methanol (1:1, v/v) and stored at –30°C. Cell-line lipids were extracted using the following steps. First, cells were mixed with 150 µL of chloroform/methanol (1:2, v/v) and 10 µL of 1 µg/mL of lipid

standards, including TG (11:1-11:1-11:1), SM (d18:1-12:0), Cer (d18:1-12:0), dCer (d18:1-12:0), So (d17:1), and Sa (d17:0) as internal standard (IS). The sample was incubated on ice for 10 min. After centrifugation (13,800 ×g, 2 min at 4 °C), 150 µL of supernatant was transferred to a new eppendorf tube. Second, the remaining pellet was resuspended in 150 µL chloroform/methanol/37% (1N) HCl (40:80:1, v/v/v) and incubated on ice for 15 min. After that, 50 µL of cold chloroform and 90 µL of cold 0.1 mol/L HCl were added to the pellet solution. After vortexing for 1 min and centrifugation at 6,500 × g for 2 min at 4 °C, the bottom organic phase was transferred to a new tube (Haag et al., 2012).

2.2.7 LC/MS conditions

Quantification of target lipids in 45 individual plasma samples was performed using 6490 Accurate-Mass Triple Quadrupole (QqQ) LC-MS coupled with a 1200 series HPLC system (Agilent Technologies, Wilmington, DE, USA) using a Hypersil GOLD column (2.1 × 100 mm ID; 1.9 µm, Thermo science). This provided high sensitivity using iFunnel technology with three components: Agilent Jet Stream technology, a hexabore capillary, and a dual ion funnel. The same solvents A and B were used for global lipid profiling. Flow rate was 0.2 mL/min. The injection volume was 2 µL for each run. The gradient elution program consisted of holding solvent (A/B: 95/5) steady for 10 min, a first linear gradient to solvent (A/B: 70/30) for 20 min, a second linear gradient to solvent (A/B: 10/90) for 10 min, and a third linear gradient to solvent (A/B: 95/5) for 1 min. The column was equilibrated with

5% solvent B for 4 min before reuse. Total run time was 45 min for each analysis. All acquisition methods used the following parameters: 3500 V positive mode of capillary voltage, 3000 V negative mode of capillary voltage, sheath gas flow of 11 L/min (UHP nitrogen) at 200ºC, drying gas flow of 15 L/min at 150ºC, and nebulizer gas flow at 25 psi. Multiple reaction monitoring (MRM) conditions, including transition and MS/MS collision energy, were optimized to analyze various lipids in different biological samples.

2.2.8 Immuno-Fluorescence staining

Cells were seeded onto 2 well-chamber slides at 7×10^3 cells/well and incubated overnight. After 24 h of incubation, slides were blocked with 3 % BSA in phosphate-buffered saline (PBS) and incubated overnight at 4 ℃ with primary antibody against LC3, α-SMA, p62, and Lamp2 (Abcam), FGF-2, and Cathepsin D (Santa Cruz Biotechnology, Santa Cruz, CA, USA). After washing three times with TTBS, slides were incubated with a secondary antibody with fluorescence, such as Alexa Fluor 488 and Alexa Fluor 555 (Life Technologies) for 1 h at room temperature. After being washed three times with PBS, images were obtained with LSM710.

2.2.9 Transmission electron microscopy (TEM)

Cells were incubated with treatment for 24 h. After washing with PBS, cells

were immediately fixed with Karnovsky's solution. After fixation, cells were stained with 0.5% aqueous uranyl acetate for 20 min, dehydrated with graded ethanol solutions, and embedded in Spurr's resin. Thin sections were cut with an ultra-microtome and stained with 2% uranyl acetate and Reynolds's lead citrate. Sections were examined using a LIBRA 120 transmission electron microscope (Carl Zeiss) at an accelerating voltage of 80 kV.

2.2.10 Monitoring Autophagic Flux

To monitoring autophagic flux, we used chloroquine, a lysosomal inhibitor. Cells were treated with 10μM chloroquine for 24 h. We compared protein, such as LC3 and p62, with chloroquine and without chloroquine.

2.2.11 Neutral lipid staining assay

Lipid droplets were measured using a HCS LipidTOX™ Red neutral lipid stain kit according to the manufacturer's protocols (Life Technologies). Briefly, cells were treated for 24 h and fixed with 4% paraformaldehyde. After washing, the cell pellet was suspended in 1X staining solution at RT for 30 min. Cells were analyzed at an excitation wavelength of 594 nm using LSM710. LD area was measured using Image J software (http://rsb.info.nih.gov/ij/).

2.2.12 Experimental co-culture set-ups for measurement of fibrosis

Co-culture plates were purchased from Corning (Corning, NY, USA). Chang cells were seeded onto the upper plate (inserts). LX-2 cells were seeded onto the bottom plate. FFA and inhibitors were used to treat Chang cells. LX-2 cell activation was determined by fibrosis. Fibrosis effect was measured using an immune-fluorescence protocol. Images were obtained using LSM710.

2.2.13 Statistical analysis

All data were expressed as mean ± standard error of the mean (SEM). Student's *t*-test was used to compare groups. Statistical significance was found when the *p* value was less than 0.05.

2.3 Results

2.3.1 FFA uptake increases sphingolipids in liver cells

We examined sphingolipids associated with FFA-induced steatosis. FFA led to an increased total level of sphingolipids and triacylglycerol (TG) (Figure 2.1B). FFA increased the levels of five kinds of sphingolipids: sphinganine (SA), dihydroceramide (dCer), ceramide (Cer), sphingosine (SO), and sphingomyelin (SM) (Figure 2.1A). As shown in the heat map of TG species, lipid profiling of some TG classes after exposure to a low concentration of FFA (31.25 μM and 62.5 μM) was similar to that after treatment with only XM462, an inhibitor of dihydroceramide desaturase (Figure 2.3A, blue square). We focused on dihydroceramide-related autophagy induction. We examined the effect of dihydroceramide using three inhibitors: ceramide synthase inhibitor Fumonisin B1, serine palmitoyl transferase inhibitor Myriocin, and dihydroceramide desaturase inhibitor XM462. The steatosis indicator TG was increased by FFA in a dose-dependent manner (Figure 2.1B). The FFA treatment had three biological replicates. Each lipid extract of these cells was also analyzed with three replicates. Using an octadecylsilyl silica column, various lipid species were separated according to their fatty acyl compositions, including different carbon numbers (CNs) and double bonds (DBs). Various lipids, including 24 Cers and 8 dCers, were analyzed successfully (Figure 2.3A-E), with several broken-line graphs describing the quantitative alteration of each species in the

dihydroceramide and ceramide class. Some species in the dihydroceramide and ceramide class were significantly increased by FFA. In dihydroceramide, d16:0-18:3, d18:0-16:0, and d18:0-20:0 were increased significantly (Figure 2.2A). The levels of several ceramide species were increased in a dose-dependent manner (Figure 2.2B and 2.2C). C16-ceramides can indicate liver injury caused by a high-fat-diet-induced steatohepatitis and insulin resistance (Raichur et al., 2014). Our results indicated that d18:1-C16:0 ceramides were increased by FFA. Dihydroceramide is a precursor of ceramide, an important regulator of cell death. C16-dihydroceramides are parallel to C16-ceramides. Therefore, the increase of C16-dihydroceramides might indicate liver injury. However, dihydroceramide related to liver damage has not been reported yet. Each lipid-class heat maps in various lipids, including 68 TGs, 13 SMs, 24 Cers, 8 dCers, 2 Sa, and 1 So, were visually analyzed (Figure 2.3A-E). Optimized MRM conditions of six lipids are listed in Table 3. Next, validation of lipid analysis based on MRM was performed to estimate the performance of lipid quantification (Table 4). Our results revealed that the levels of sphingolipids and TG could be increased by FFA-induced autophagosome accumulation. We observed cell morphology after treatment of FFA by transmission electron microscopy (TEM). TEM images revealed an increase in the number of LD in FFA-dose-dependent cells (Figure 2.1C). Also, cell viability and ATP production showed a similar pattern (Figure 2.1D). We chose a concentration of FFA because 500μM is an appropriate concentration for the steatosis model, which has the highest production of triacylglycerol and did not impact cell viability and ATP production.

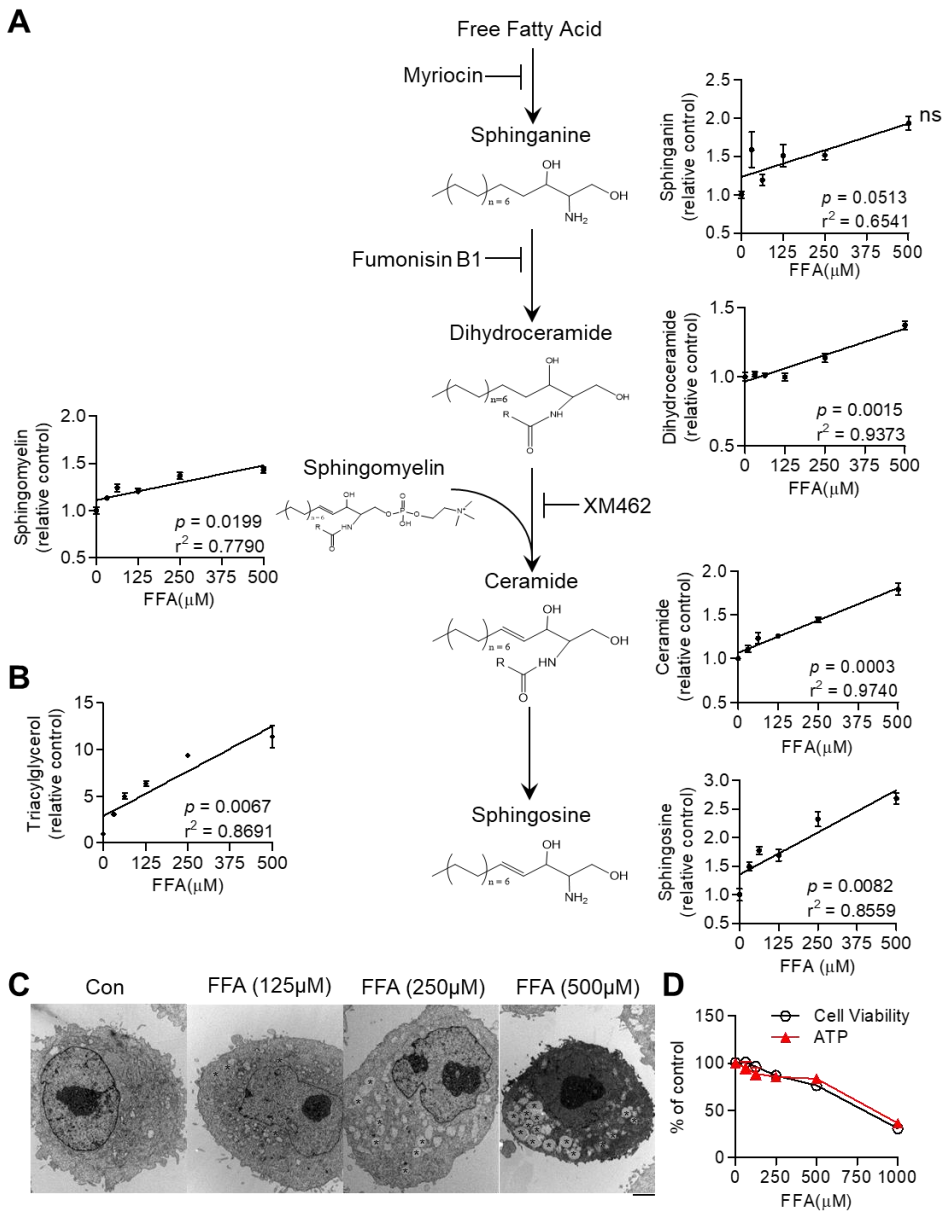

Figure 2.1. FFA uptake increases sphingolipids in liver cell

Lipid profiling analysis was performed using the constructed MRM method to determine the quantitative alteration of various lipids in Chang cells treated by FFA

at different concentrations (31.5, 62.5, 125, 250, and 500 μM). (A) Total sphingolipids contents, (B) Total TG contents. Data were expressed as mean ± SEM. (C) Lipid droplets (LD) on cell morphology by TEM analysis. (D) Cell viability and ATP production according to FFA concentration.

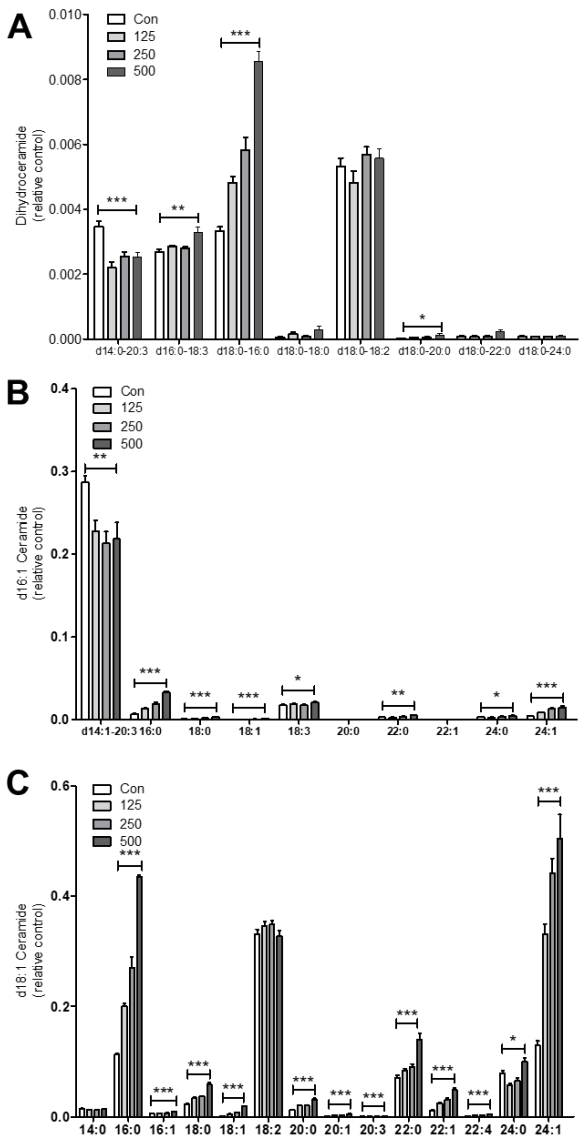

Figure 2.2. Various lipid species were separated according to their fatty acyl compositions, including different carbon numbers (CNs) and double bonds (DBs)

(A) Dihydroceramide class, (B) d14:1 and d16:1 ceramide class, (C) d18:1 ceramide class. Data were expressed as mean ± SEM. * Significantly different from the control ($p < 0.05$), **Significantly different from the control ($p < 0.01$), ***Significantly different from the control ($p < 0.001$).

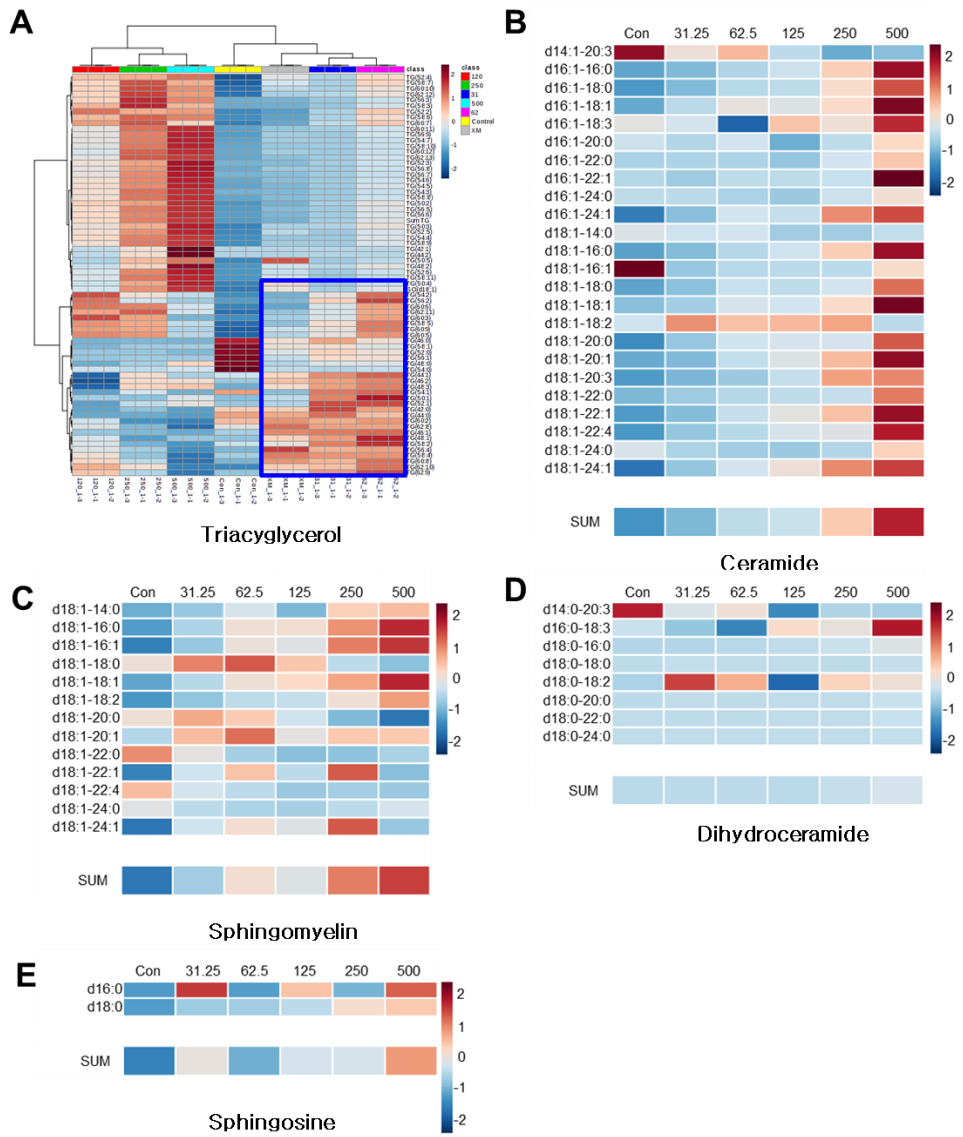

Figure 2.3. Heat maps of FFA-accumulation cells

Heat maps depicting lipid expression change. (A) Triglycerol, (B) ceramide, (C) sphingomyelin, (D) dihydroceramide, (E) sphingosine level. Blue, white, and red represent lipid levels

Table 3. List of optimized MRM conditions for six lipids

Lipids	Ion mode	MRM transitions	MS/MS CE (eV)
TG	Positive	$[M+NH_4] > [M+NH_4–RCOONH_4]$	18
SM	Positive	[M+H] > 184	30
Cer	Positive	[M+H] > 264 [a] or 236 [b]	26
dCer	Positive	[M+H] > 266	26
So	Positive	[M+H] > [M+H–18]	10
Sa	Positive	[M+H] > [M+H–18]	10

Table 4. Validation of lipid analysis based on MRM to estimate the performance of lipid quantification

Lipids	RT (min)	RSD (n=9) (%)		Correlation (R^2)	Linear range (pg)	LOD (pg)
		RT	Peak area			
TG	4.2	1.1	5.7	0.9992	0.1 – 2000	0.1
SM	3.69	1.0	5.5	0.9956	1 – 2000	1
Cer	3.52	1.0	6.3	0.9962	1 – 2000	1
dCer	3.85	1.5	6.9	0.9984	1 – 2000	1
So	1.39	0.9	3.4	0.9803	10 – 2000	10
Sa	1.46	1.4	4.2	0.9984	10 – 2000	10

2.3.2 FFA led to autophagosome formation

FFA induced autophagy in a dose-dependent manner in human liver Chang cells (Figure 2.4A). We established FFA-induced autophagy by assessing the levels of LC3-II and p62/SQSTM1 (p62). Actually, p62 is degraded by autophagy, but in Figure 2.4A, p62 were increased in a dose-dependent manner. FFA is caused by blocks of the fusion of autophagosomes with lysosomes, leading to an accumulation of autophagosomal structure (Bjorkoy et al., 2005). These results were reconfirmed

by densitometry analysis (Figure 2.4B). LC3 puncta was performed to measure the level of LC3-II. Increase of the number of LC3 puncta was used to monitor the autophagic process (Zhang et al., 2013). These results were reconfirmed by LC3 puncta counting (Figure 2.4C and 2.4D). Also, the fluorescence intensity of autophagosomes was measured (Figure 2.4E). Taken together, these results support the idea that FFA can induce autophagosome formation.

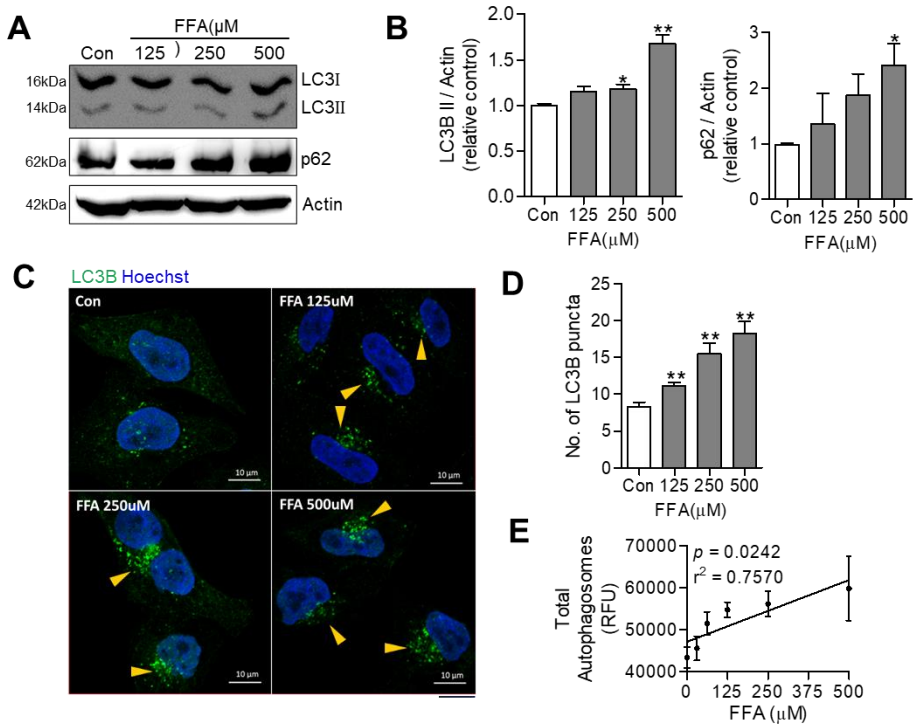

Figure 2.4. FFA leads to autophagosome formation and increased dihydroceramide by FFA correlates with autophagosome accumulation

(A) Protein levels of LC3 and p62/SQSTM1 in Chang cells. LC3- II and

p62/SQSTM1 levels were increased in a dose-dependent manner. (B) Densitometry analysis of each protein level ($n = 3$). (C) LC3 puncta image staining with LC3. Scale bars: 10 μm. (D) Number of LC3 puncta using Image J software. (E) Measurement of autophagosomes using autophagosome fluorescence detection kit ($n = 3$).
Data were expressed as mean ± SEM. * Significantly different from the control ($p < 0.05$), **significantly different from the control ($p < 0.01$).

2.3.3 Dihydroceramide product correlates with autophagosome accumulation

According to the response to FFA concentration, we assessed the correlation of autophagosome formation-related protein, such as LC3 and p62, with lipid metabolism, such as dihydroceramide, ceramide, and triacylglycerol (Figure 2.5). FFA-induced increase of dihydroceramide was correlated with autophagosome accumulation, such as the level of p62 and LC3-II. Triacylglycerol was not correlated with p62 and LC3-II. Ceramide was correlated with p62, but not with LC3-II. Therefore, dihydroceramide has the most important role in accumulation of autophagosomes.

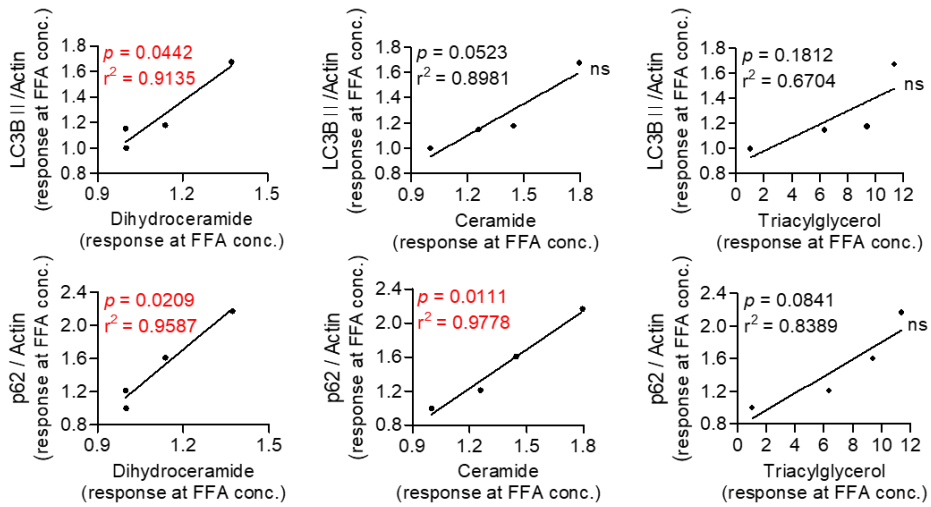

Figure 2.5. Dihydroceramide product correlates with autophagosome accumulation

Dihydroceramide product correlates with autophagosome accumulation.

2.3.4 Dihydroceramide, a ceramide precursor, stimulates autophagy in the perinuclear region

It has been reported that XM462 can induce an increase of dihydroceramide by inhibiting dihydroceramide desaturase (Munoz-Olaya et al., 2008). Dihydroceramide was increased by XM462 (Figure 2.6A). Therefore, we evaluated the effect of various inhibitors on sphingolipids. Autophagosome formation was measured after co-treatment with FFA and different inhibitors. Autophagosome activity was increased by FFA or XM462 with FFA. However, myriocin and fumonisin B1 inhibited FFA-induced autophagosome formation (Figure 2.6B). Co-

treatment with FFA and XM462 increased autophagosome formation even more than did treatment of myriocin or fumonisin B1 with FFA. LC3 puncta were used to monitor autophagosomes (Figure 2.6C). Our results revealed that dihydroceramide was parallel to autophagosome formation. Cell morphology after treatment of FFA with sphingolipid inhibitors was also examined. Co-treated FFA and XM462 cells were subjected to analysis for LD and autophagic vacuoles, such as autolysomes and autophagosomes. It was found that myriocin and fumonisin B1 decreased LD and autophagic vesicles more than did treatment with FFA and XM462 (Figure 2.6D).

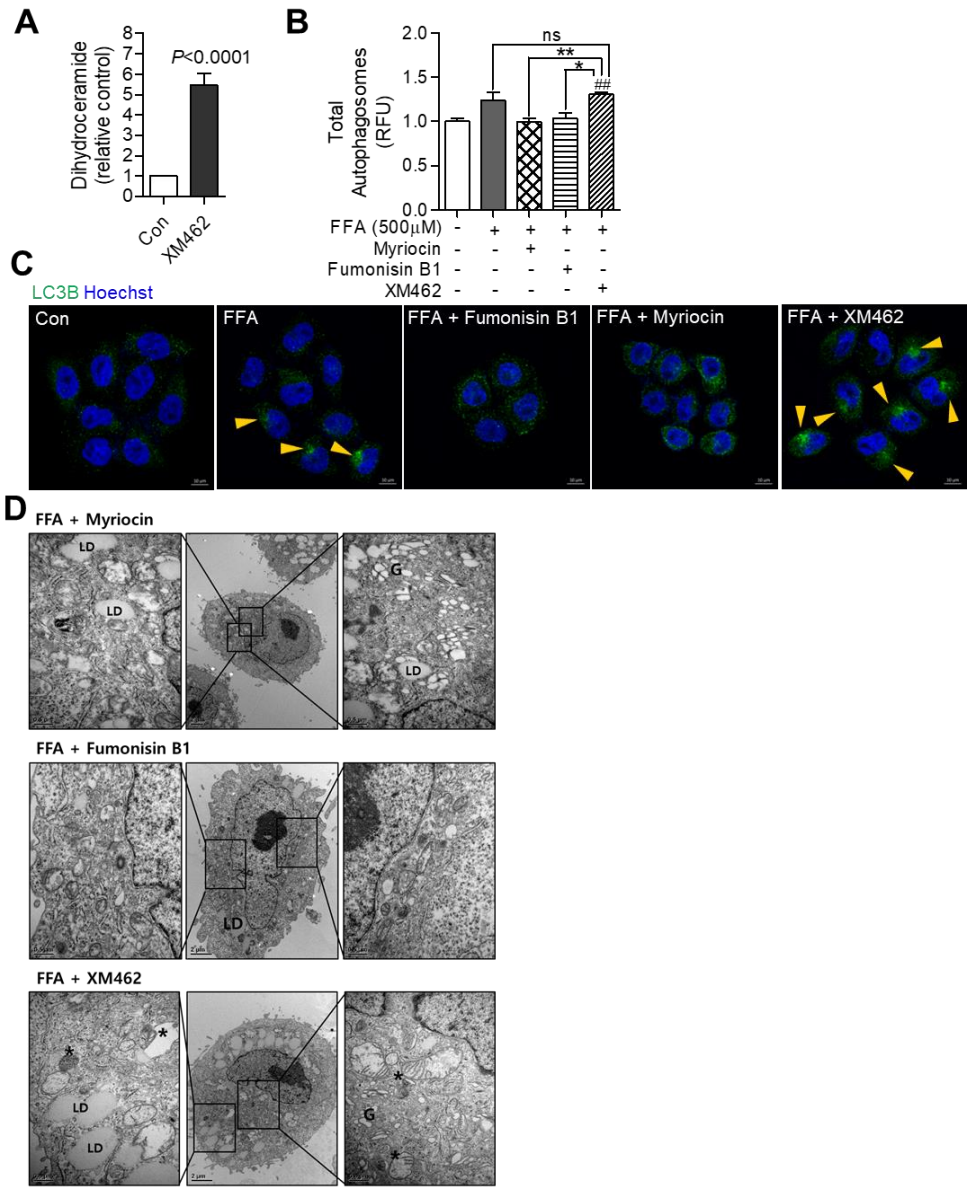

Figure 2.6. Dihydroceramide, a ceramide precursor, stimulates autophagy in the perinuclear region

(A) Dihydroceramide was increased by XM462, dihydroceramide desaturase inhibitor (B) Quantitation of autophagosomes after treatment with various

sphingolipid inhibitors (n = 3). (C) the LC3 puncta image was obtained using LC3-II staining. Scale bars: 10 μm. (D) TEM images of sphingolipid metabolism with FFA. The box in the middle panel and the corresponding magnification image indicated autophagic vacuoles and lipid droplets. Insets showing lipid droplets (LD), and golgi (G). *indicating autophagic vacuoles. Scale bars: 2 and 0.5 μm. Data were expressed as mean ± SEM. * Significantly different from XM462 ($p < 0.05$), **significantly different from XM462 ($p < 0.01$), ##significantly different from the control ($p < 0.01$).

2.3.5 Dihydroceramide impairs autophagic flux and increases lipid droplets

Autophagic flux was assessed by the co-localization of Cathepsin D and Lamp2 with p62/SQSTM1 after the production of dihydroceramide (Figure 2.7A and 2.7B). The adapter protein p62/SQSTM1 has an important role in the regulation of several key signaling pathways. It helps transport ubiquitinated proteins to autophagosomes and proteasomes for degradation (Trocoli et al., 2014). Thus, accumulation of p62 can be used to monitor autophagic flux. FFA and XM462 with FFA were co-localized with p62, cathepsin D, and Lamp2. FFA and XM462 with FFA increased the levels of p62 and Lamp2. In the normal autophagic process, autophagosomes will mature and fuse with lysosomes to form autolysosomes, followed by degradation (Xie et al., 2010). However, blockage of utophagosomes

and lysosomes will impair autophagosomal degradation. Increased dihydroceramide blocked autophagosome (LC3) and lysosome (Lamp2) fusion. FFA and XM462 with FFA were not co-localized with LC3 and Lamp2 (Figure 2.8). Therefore, LC3 and Lamp2 were not fused after the increase of dihydroceramide. Moreover, we monitored autophagic flux in the chloroquine state. Chloroquine is a lysosomal inhibitor agent that impairs lysosomal acidification. LC3-II accumulates even under normal conditions, because the turnover of LC3-II by basal autophagy is blocked (Solomon et al., 2003). FFA and XM462 with FFA accumulated more LC3 and p62 in the chloroquine state than in the basal state (Figure 2.7C). Taken together, these results suggest that an increase in the dihydroceramide level could cause a defect in the autophagic flux, causing protein aggregation. In addition, impairment of autophagic flux could induce increases in triglyceride (TG) storage in lipid droplets (LD). Furthermore, increased dihydroceramide increased TG level and LD formation (Figure 2.9A and 2.9B). The LD area of XM462 with FFA was significantly increased compared to that of FFA with other inhibitor groups.

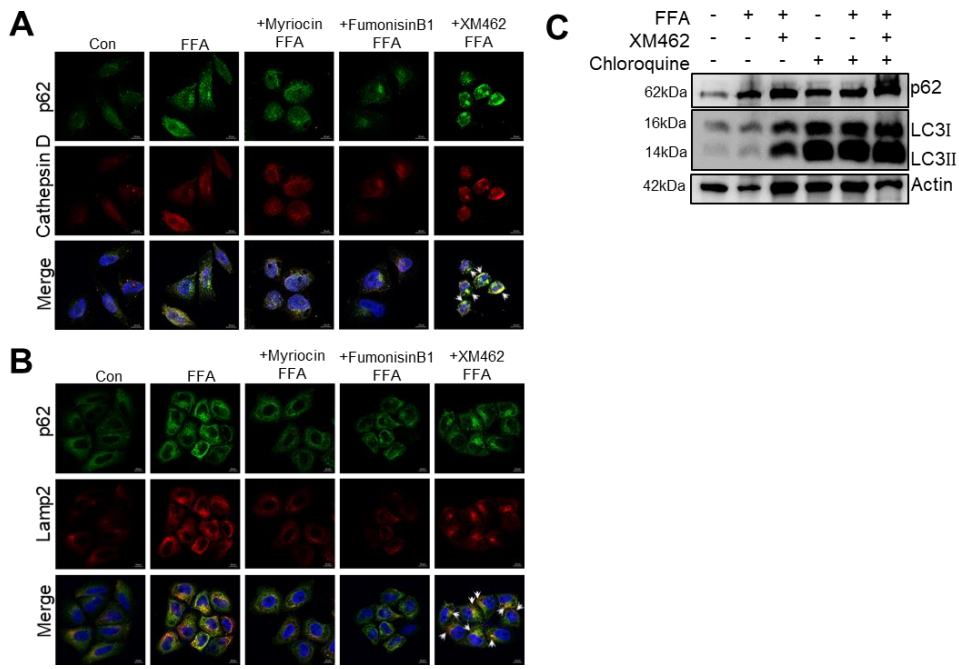

Figure 2.7. Dihydroceramide-induced autophagic flux dysfunction

Representative confocal images showing autophagosomal-lysosome fusion. Impairment of autophagic flux increased p62-lysosome fusion and blocked LC3-lysosome fusion. (A) Co-localization image of cathepsin D (red, lysosome) and p62/SQSTM1 (green, autophagy flux). (B) Co-localization image of Lamp2 (red, lysosome) and p62/SQSTM1 (green, autophagy flux). Scale bars: 10 μm. (C) FFA and XM462 with FFA were more accumulated more LC3 and p62 in the chloroquine state than in the basal state.

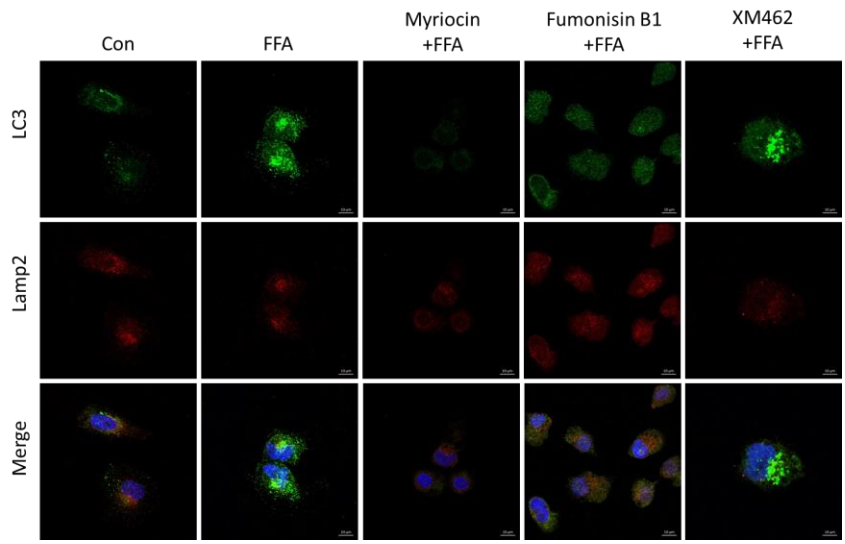

Figure 2.8. Dihydroceramide impairs autophagic flux

Co-localization image of LC3 (green, autophagosome) and Lamp2 (red, lysosome). Scale bars: 10 μm.

2.3.6 Rapamycin alleviates LD formation by dihydroceramide

Rapamycin prevented LD formation (Figure 2.9A and 2.9B). FFA and XM462 with FFA decreased the LD area significantly after treatment with rapamycin (Figure 2.9A and 2.9B). We assessed the LD area by staining the neutral lipid followed by differential interference contrast (DIC) imaging. Therefore, our data showed dihydroceramide increased the LD area and autophagosome accumulation by FFA uptake (Figure 2.9C).

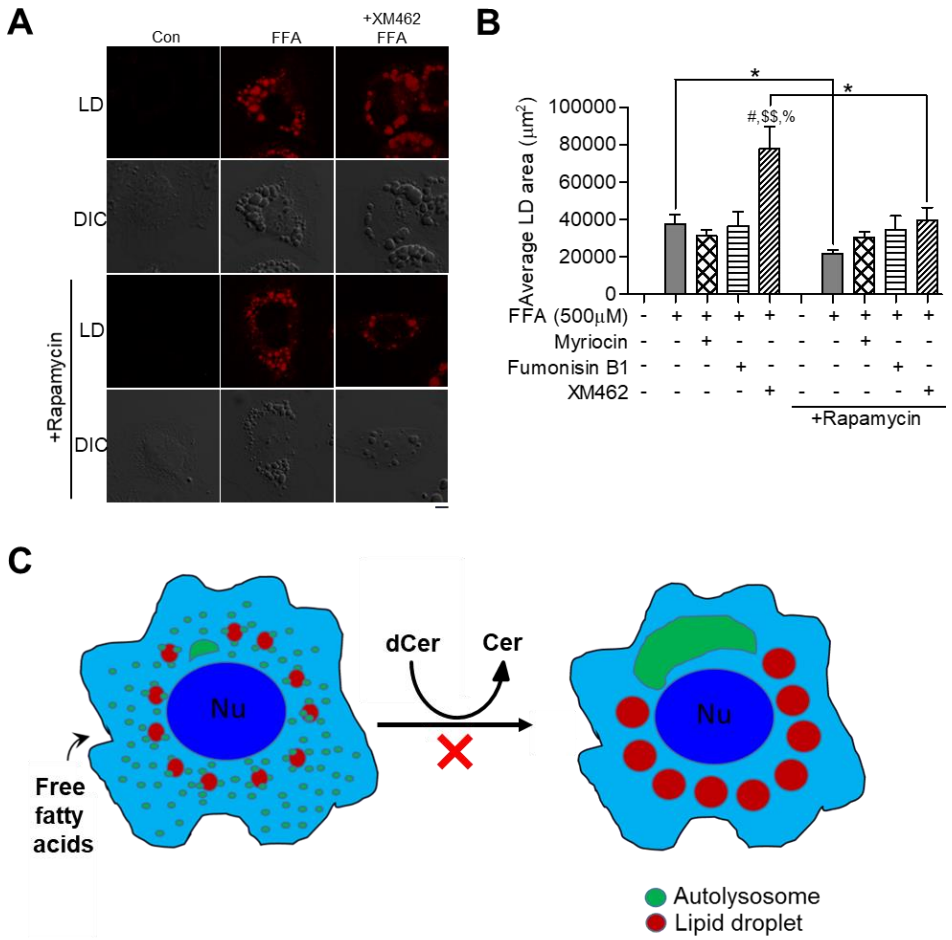

Figure 2.9. Rapamycin alleviates LD formation by dihydroceramide

(A) LD staining (red) and DIC image, (B) Average LD area (μm^2), (C) Scheme showed dihydroceramide increased LD area and autophagosome accumulation by FFA uptake. Data were expressed as mean ± SEM. $^{\#}$ Significantly different from FFA ($p < 0.05$), $^{\$\$}$ significantly different from Myriocin with FFA ($p < 0.01$), $^{\%}$ significantly different from Fumonisin B1 with FFA ($p < 0.05$), *significantly different from each group ($p < 0.05$). Scale bars: 10 μm.

2.3.7 Rapamycin recuperates fibrosis by recovering autophagic flux by increased dihydroceramide

Treatment with FFA and XM462 with FFA resulted in the accumulation of p62. This effect was similar to the blockade of autophagic flux induced by chloroquine or bafilomycin A1. (Rossi et al., 2009) However, rapamycin reduced the level of p62 (Figure 2.10A). In this study, we investigated fibrosis by co-culturing Chang liver cells and LX-2 cells (liver hepatic stellate cells, HSCs). We examined fibrosis marker α-smooth muscle actin (α-SMA) and basic fibroblast-growth factor (FGF-2) by dihydroceramide in co-cultured Chang cells and LX-2 cells. The fibrosis level was increased when dihydroceramide was increased. Both FFA and XM462 with FFA increased the levels of FGF-2 and α-SMA. However, myriocin and fumonisin B1 with FFA group were not increased. Myriocin and fumonisin B1 decreased FFA-induced upregulation of α-SMA and FGF-2. In the rapamycin treatment group, FFA and XM462 with FFA prevented the upregulation of α-SMA and FGF-2. Rapamycin recovered the fibrosis effect on α-SMA and FGF-2 induced by FFA (Figure 2.10B).

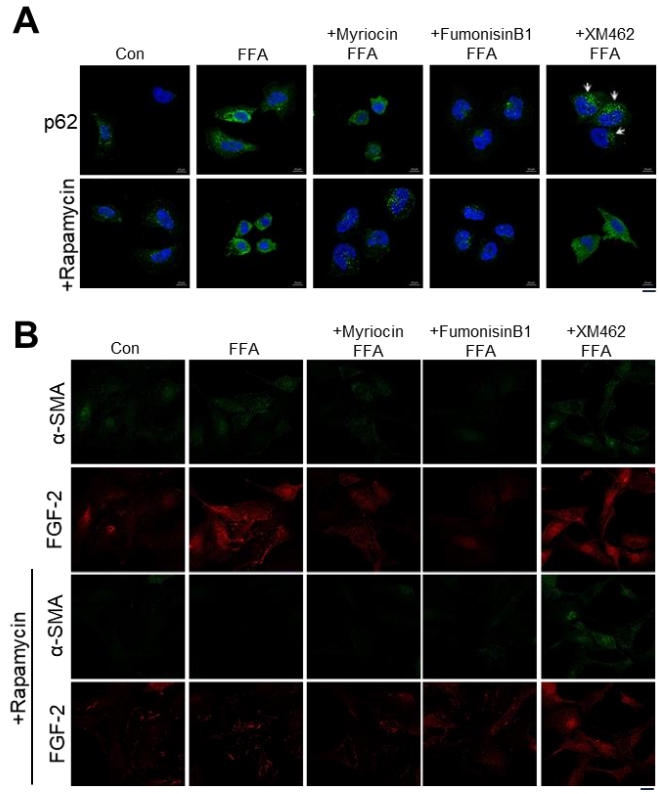

Figure 2.10. Rapamycin recuperates LD accumulation and fibrosis by recovering autophagic flux

(A) Analysis of p62/SQSTM1 in immuno-fluorescence staining treated with or without rapamycin. (B) α-SMA and FGF-2 fluorescence expression in co-culture between LX-2 cells and Chang cells with or without rapamycin.

2.4 Discussion

Autophagy is important for liver homeostasis. Autophagy may prevent the progression of steatosis in NAFLD (Codogno and Meijer, 2013). However, autophagy deficiency may accelerate NASH characterized by chronic liver injury, inflammation, and fibrosis (Ma et al., 2013). It has been shown that the activation of autophagic flux can decrease the expression of p62. Accumulation of p62 reflects a blockage in the autophagic flux. Although p62 levels and polyubiquitinated proteins are commonly increased in cells showing deficiency in the autophagic process, there are studies also showing changed LC3-II in autophagy (Zhang et al., 2013; Gonzalez-Rodriguez et al., 2014). Levels of p62 are known to be markedly elevated in atherosclerotic plaques, suggesting that this aggregate can also mediate cellular toxicity, apoptosis, and inflammasome activation in other disease conditions where protein aggregation occurs (Sergin and Razani, 2014). Our results revealed that FFA could lead to autophagosome accumulation and increased p62 and LC3-II levels. Dihydroceramide also induced up-regulation of p62 and LC3-II, as is similar to results of previous studies (Signorelli et al., 2009; Gagliostro et al., 2012; Li et al., 2014). However, an increased level of LC3-II or accumulation of GFP-LC3 puncta is not always an indication of autophagy induction. They may represent a blockade in autophagosome maturation (Zhang et al., 2013). It has been reported that newly formed autophagosomes induced by dihydroceramide are not rapidly cleared by

fusion with lysosomes. On the other hand, dihydroceramide aggravated autophagy flux. We investigated whether an increase or decrease of dihydroceramide could regulate autophagy. Our study suggested that an increase of dihydroceramide by XM462 with FFA obstructed the autophagy flux, consequently causing fibrosis.

It has been recently indicated that sphingolipids have many functions in various biological processes (Li et al., 2014). In this study, we investigated whether dihydroceramide could regulate autophagy in FFA accumulation. We showed that FFA treatment in human liver cells could lead to autophagosome accumulation and cause marked accumulation of sphinganine, dihydroceramide, ceramide, sphingosine, and sphingomyelin, important sphingolipids in a *de novo* biosynthesis pathway.

NAFLD begins with an abnormal accumulation of TG, which might be a potential mechanism of liver injury in NASH (Ibrahim et al., 2011). NASH is characterized by abnormal lipid metabolism and the accumulation of TG storage in LD of hepatocytes. The accumulation of lipids can initiate NASH (Song et al., 2014). Accumulation of TG in liver cells has been considered as a critical pathogenic trigger in the development of NAFLD (Fon Tacer and Rozman, 2011). Consistent with these reports, our results also revealed that FFA overloading in cells induced an increase of TG storage in lipid droplets (LD), causing fibrosis. Increase in dihydroceramide amplified LD formation, subsequently causing the activation of HSCs. We found that increases in dihydroceramide were associated with each TG class level. Therefore, dihydroceramide is a meaningful marker in NAFLD initiation. HSCs are well-known

major fibrogenic cells in livers. They are filled with cytoplasmic LD before being activated. We observed the fibrogenic effect using a co-culture system of Chang cells and LX-2 cells. Fibrosis markers, such as α-SMA and FGF-2, were increased in LX-2 cells.

It has been reported that rapamycin can inhibit mTOR and recover autophagic flux by decreasing p62 and the accumulation of autophagosomes, thus ameliorating a saturated fatty-acid-induced increase in apoptotic cells (Gonzalez-Rodriguez et al., 2014). Treatment with rapamycin, an activator of autophagy, has been reported to significantly decrease LD but increase the co-localization of LC3 and Lamp1 (Singh et al., 2009; Liu and Czaja, 2013). Moreover, upregulated autophagy by rapamycin can effectively reduce AT mutant Z gene aggregation in hepatocytes with the reduction of hepatocellular injury markers and the level of hepatic fibrosis (Song et al., 2014). These findings suggest that autophagy plays a protective role in the pathology of liver disease. It can reduce hepatic fibrosis (Song et al., 2014). We found that rapamycin prevented the impairment of autophagic flux by decreasing p62. Therefore, rapamycin might be a scavenger for fibrosis in NAFLD. The LD area was also decreased by rapamycin. Further studies are necessary to examine the relationship between dihydroceramide and NAFLD *in vivo*. Additional studies are required to better understand the role of autophagy in the liver and in specific liver cells in NAFLD (Lavallard and Gual, 2014).

GENERAL CONCLUSION

Ephedrine induces mitochondrial damage through oxidative stress and depolarization in LX-2 cells. ROS generation and MMP depletion can cause PINK1-Parkin activated mitophagy, which may be a one of the major mechanisms for ephedrine-induced liver injury. More detailed *in vitro* mechanism study and *in vivo* studies are necessary to examine the mechanism of ephedrine-induced liver toxicity. Our findings suggest that ephedrine causes liver toxicity via mitochondrial damage and subsequent execessive mitophagy. Parkin is a key protein for the regulation of ephedrine-induced mitophagy in the liver cell line. Also, antioxidants could be a therapeutic strategy for the treatment of disease caused by ephedrine. Therefore, the regulation of Parkin could provide novel therapeutic opportunities to prevent ephedrine-induced mitochondrial damage.

Also, this study demonstrated that dihydroceramide could regulate autophagy. Accumulation of dihydroceramide inhibited the autophagic flux in FFA-mediated lipid accumulation in Chang cells. Impairment of the autophagic flux resulted in progression of fibrosis. In addition, rapamycin reduced hepatic fibrosis by up-regulating dihydroceramide. These findings strongly suggest that the recovery of autophagy flux can regulate the progression of NAFLD and that dihydroceramide might be used as a new diagnostic target for NAFLD.

In conclusion, this study evaluated hepatotoxicity through impaired autophagic flux. Therefore, these results strongly suggest that therapies aimed to restore the autophagic flux might prevent or attenuate the progression of NAFLD.

REFERENCES

Alkhouri N and Mccullough AJ (2012). Noninvasive Diagnosis of NASH and Liver Fibrosis Within the Spectrum of NAFLD. Gastroenterology & Hepatology 8(10): 661-668.

Bedia C, Levade T and Codogno P (2011). Regulation of Autophagy by Sphingolipids. Anti-Cancer Agents in Medicibal chemistry 11(9): 844-853.

Bjorkoy G, Lamark T, Brech A, Outzen H, Perander M, Overvatn A, Stenmark H and Johansen T (2005). p62/SQSTM1 forms protein aggregates degraded by autophagy and has a protective effect on huntingtin-induced cell death. J Cell Biol 171(4): 603-614.

Chen KK and Schmidt CF (1926). The action and clinical use of ephedrine: An alkaloid isolated from the chinese drug ma huang. Journal of the American Medical Association 87(11): 836-842.

Codogno P and Meijer AJ (2013). Autophagy in the liver. J Hepatol 59(2): 389-391.

Czaja MJ, Ding WX, Donohue TM, Jr., Friedman SL, Kim JS, Komatsu M,

Lemasters JJ, Lemoine A, Lin JD, Ou JH, Perlmutter DH, Randall G, Ray RB, Tsung A and Yin XM (2013). Functions of autophagy in normal and diseased liver. Autophagy 9(8): 1131-1158.

Dunnick JK, Kissling G, Gerken DK, Vallant MA and Nyska A (2007). Cardiotoxicity of Ma Huang/caffeine or ephedrine/caffeine in a rodent model system. Toxicologic Pathology 35(5): 657-664.

Eid N, Ito Y and Otsuki Y (2015). Mitophagy in steatotic hepatocytes of ethanol-treated wild-type and Parkin knockout mice. Am J Physiol Gastrointest Liver Physiol 309(6): G513-514.

Evans TD, Sergin I, Zhang X and Razani B (2017). Target acquired: Selective autophagy in cardiometabolic disease. Science Signaling 10(468): eaag2298.

Feyza Gunduz FMA, Partha K Chandra, Sidhartha Hazari, Bret Poat, Darren P Baker, Luis a Balart and Srikanta Dash (2012). Free fatty acids induce ER stress and block antiviral activity of interferon alpha against hepatitis C virus in cell culture. Virology Journal 9(143).

Fon Tacer K and Rozman D (2011). Nonalcoholic Fatty liver disease: focus on lipoprotein and lipid deregulation. J Lipids 2011: 783976.

Gagliostro V, Casas J, Caretti A, Abad JL, Tagliavacca L, Ghidoni R, Fabrias G and Signorelli P (2012). Dihydroceramide delays cell cycle G1/S transition via activation of ER stress and induction of autophagy. International Journal of Biochemistry & Cell Biology 44(12): 2135-2143.

Giraudi PJ, Becerra VJ, Marin V, Chavez-Tapia NC, Tiribelli C and Rosso N (2015). The importance of the interaction between hepatocyte and hepatic stellate cells in fibrogenesis induced by fatty accumulation. Exp Mol Pathol 98(1): 85-92.

Gomez-Lechon MJ, Donato MT, Martinez-Romero A, Jimenez N, Castell JV and O'connor JE (2007). A human hepatocellular in vitro model to investigate steatosis. Chem Biol Interact 165(2): 106-116.

Gonzalez-Rodriguez A, Mayoral R, Agra N, Valdecantos MP, Pardo V, Miquilena-Colina ME, Vargas-Castrillon J, Lo Iacono O, Corazzari M, Fimia GM, Piacentini M, Muntane J, Bosca L, Garcia-Monzon C, Martin-Sanz P and Valverde AM (2014). Impaired autophagic flux is associated with increased endoplasmic reticulum stress during the development of NAFLD. Cell Death & Disease 5.

Haag M, Schmidt A, Sachsenheimer T and Brugger B (2012). Quantification of Signaling Lipids by Nano-Electrospray Ionization Tandem Mass Spectrometry

(Nano-ESI MS/MS). Metabolites 2(1): 57-76.

Hamacher-Brady A and Brady NR (2015). Mitophagy programs: mechanisms and physiological implications of mitochondrial targeting by autophagy. Cell Mol Life Sci.

Ibrahim SH, Kohli R and Gores GJ (2011). Mechanisms of Lipotoxicity in NAFLD and Clinical Implications. Journal of Pediatric Gastroenterology and Nutrition: 1.

Lavallard VJ and Gual P (2014). Autophagy and non-alcoholic fatty liver disease. Biomed Res Int 2014: 120179.

Lee AY, Jang Y, Hong SH, Chang SH, Park S, Kim S, Kang KS, Kim JE and Cho MH (2017). Ephedrine-induced mitophagy via oxidative stress in human hepatic stellate cells. The Journal of Toxicological Sciences 42(4): 461-473.

Lee AY, Lee JW, Kim JE, Mock HJ, Park S, Kim S, Hong SH, Kim JY, Park EJ, Kang KS, Kim KP and Cho MH (2017). Dihydroceramide is a key metabolite that regulates autophagy and promotes fibrosis in hepatic steatosis model. Biochem Biophys Res Commun 494(3-4): 460-469.

Li L, Hai J, Li Z, Zhang Y, Peng H, Li K and Weng X (2014). Resveratrol modulates autophagy and NF-kappaB activity in a murine model for treating non-alcoholic fatty liver disease. Food Chem Toxicol 63: 166-173.

Li Y, Li S, Qin X, Hou W, Dong H, Yao L and Xiong L (2014). The pleiotropic roles of sphingolipid signaling in autophagy (vol 5, pg e1245, 2014). Cell Death & Disease 5.

Lin CW, Zhang H, Li M, Xiong X, Chen X, Chen X, Dong XC and Yin XM (2013). Pharmacological promotion of autophagy alleviates steatosis and injury in alcoholic and non-alcoholic fatty liver conditions in mice. J Hepatol 58(5): 993-999.

Liu AG, Smith SR, Fujioka K and Greenway FL (2013). The effect of leptin, caffeine/ephedrine, and their combination upon visceral fat mass and weight loss. Obesity (Silver Spring) 21(10): 1991-1996.

Liu K and Czaja MJ (2013). Regulation of lipid stores and metabolism by lipophagy. Cell Death Differ 20(1): 3-11.

Lorbek G and Rozm D (2012). Cholesterol and Inflammation at the Crossroads of Non-Alcoholic Fatty Liver Disease (NAFLD) and Atherogenesis. Atherogenesis.

Ma D, Molusky MM, Song J, Hu CR, Fang F, Rui C, Mathew AV, Pennathur S, Liu F, Cheng JX, Guan JL and Lin JD (2013). Autophagy deficiency by hepatic FIP200 deletion uncouples steatosis from liver injury in NAFLD. Mol Endocrinol 27(10): 1643-1654.

Malhi H and Gores GJ (2008). Molecular mechanisms of lipotoxicity in nonalcoholic fatty liver disease. Semin Liver Dis 28(4): 360-369.

Mao Y, Yu F, Wang J, Guo C and Fan X (2016). Autophagy: a new target for nonalcoholic fatty liver disease therapy. Hepat Med 8: 27-37.

Martin S and Parton RG (2006). Lipid droplets: a unified view of a dynamic organelle. Nat Rev Mol Cell Biol 7(5): 373-378.

Mizushima N, Yoshimori T and Levine B (2010). Methods in Mammalian Autophagy Research. Cell 140(3): 313-326.

Munoz-Olaya JM, Matabosch X, Bedia C, Egido-Gabas M, Casas J, Llebaria A, Delgado A and Fabrias G (2008). Synthesis and biological activity of a novel inhibitor of dihydroceramide desaturase. ChemMedChem 3(6): 946-953.

Neuschwander-Tetri BA (2010). Hepatic lipotoxicity and the pathogenesis of nonalcoholic steatohepatitis: the central role of nontriglyceride fatty acid metabolites. Hepatology 52(2): 774-788.

Ofosu A, Ramai D and Reddy M (2018). Non-alcoholic fatty liver disease: controlling an emerging epidemic, challenges, and future directions. Ann

Gastroenterol 31(3): 288-295.

Park EJ, Lee AY, Chang SH, Yu KN, Kim JH and Cho MH (2014). Role of p53 in the cellular response following oleic acid accumulation in Chang liver cells. Toxicol Lett 224(1): 114-120.

Park EJ, Lee AY, Park S, Kim JH and Cho MH (2014). Multiple pathways are involved in palmitic acid-induced toxicity. Food Chem Toxicol 67: 26-34.

Puche JE, Saiman Y and Friedman SL (2013). Hepatic stellate cells and liver fibrosis. Compr Physiol 3(4): 1473-1492.

Raichur S, Wang ST, Chan PW, Li Y, Ching J, Chaurasia B, Dogra S, Ohman MK, Takeda K, Sugii S, Pewzner-Jung Y, Futerman AH and Summers SA (2014). CerS2 haploinsufficiency inhibits beta-oxidation and confers susceptibility to diet-induced steatohepatitis and insulin resistance. Cell Metab 20(4): 687-695.

Reuben A, Koch DG, Lee WM and Acute Liver Failure Study G (2010). Drug-induced acute liver failure: results of a U.S. multicenter, prospective study. Hepatology 52(6): 2065-2076.

Rossi M, Munarriz ER, Bartesaghi S, Milanese M, Dinsdale D, Guerra-Martin MA,

Bampton ET, Glynn P, Bonanno G, Knight RA, Nicotera P and Melino G (2009). Desmethylclomipramine induces the accumulation of autophagy markers by blocking autophagic flux. J Cell Sci 122(Pt 18): 3330-3339.

Schaffer JE (2003). Lipotoxicity: when tissues overeat. Curr Opin Lipidol 14(3): 281-287.

Schmitt GC, Arbo MD, Lorensi AL, Maciel ES, Krahn CL, Mariotti KC, Dallegrave E, Leal MB and Limberger RP (2012). Toxicological Effects of a Mixture Used in Weight Loss Products: p-Synephrine Associated With Ephedrine, Salicin, and Caffeine. International Journal of Toxicology 31(2): 184-191.

Sergin I and Razani B (2014). Self-eating in the plaque: what macrophage autophagy reveals about atherosclerosis. Trends Endocrinol Metab 25(5): 225-234.

Signorelli P, Munoz-Olaya JM, Gagliostro V, Casas J, Ghidoni R and Fabrias G (2009). Dihydroceramide intracellular increase in response to resveratrol treatment mediates autophagy in gastric cancer cells. Cancer Letters 282(2): 238-243.

Singh R, Kaushik S, Wang Y, Xiang Y, Novak I, Komatsu M, Tanaka K, Cuervo AM and Czaja MJ (2009). Autophagy regulates lipid metabolism. Nature 458(7242): 1131-1135.

Sinha RA and Yen PM (2016). Thyroid hormone-mediated autophagy and mitochondrial turnover in NAFLD. Cell Biosci 6: 46.

Solomon JC, Sharma K, Wei LX, Fujita T and Shi YF (2003). A novel role for sphingolipid intermediates in activation-induced cell death in T cells. Cell Death and Differentiation 10(2): 193-202.

Song Y, Zhao Y, Wang F, Tao L, Xiao J and Yang C (2014). Autophagy in hepatic fibrosis. Biomed Res Int 2014: 436242.

Thiele C and Spandl J (2008). Cell biology of lipid droplets. Curr Opin Cell Biol 20(4): 378-385.

Trocoli A, Bensadoun P, Richard E, Labrunie G, Merhi F, Schlafli AM, Brigger D, Souquere S, Pierron G, Pasquet JM, Soubeyran P, Reiffers J, Segal-Bendirdjian E, Tschan MP and Djavaheri-Mergny M (2014). p62/SQSTM1 upregulation constitutes a survival mechanism that occurs during granulocytic differentiation of acute myeloid leukemia cells. Cell Death Differ 21(12): 1852-1861.

Wang K (2015). Autophagy and apoptosis in liver injury. Cell Cycle 14(11): 1631-1642.

Wang Y, Ding WX and Li T (2018). Cholesterol and bile acid-mediated regulation of autophagy in fatty liver diseases and atherosclerosis. Biochim Biophys Acta 1863(7): 726-733.

Williams JA and Ding WX (2015). A Mechanistic Review of Mitophagy and Its Role in Protection against Alcoholic Liver Disease. Biomolecules 5(4): 2619-2642.

Williams JA and Ding WX (2015). Targeting Pink1-Parkin-mediated mitophagy for treating liver injury. Pharmacol Res 102: 264-269.

Williams JA, Ni HM, Ding Y and Ding WX (2015). Parkin regulates mitophagy and mitochondrial function to protect against alcohol-induced liver injury and steatosis in mice. American Journal of Physiology-Gastrointestinal and Liver Physiology 309(5): G324-G340.

Xie R, Nguyen S, Mckeehan WL and Liu L (2010). Acetylated microtubules are required for fusion of autophagosomes with lysosomes. BMC Cell Biol 11: 89.

Young MM, Kester M and Wang H-G (2013). Sphingolipids: regulators of crosstalk between apoptosis and autophagy. Journal of Lipid Research 54(1): 5-19.

Zhang H, Maguire D, Swarts S, Sun W, Yang S, Wang W, Liu C, Zhang M, Zhang

D, Zhang L, Zhang K, Keng P, Zhang L and Okunieff P (2009). Replication of murine mitochondrial DNA following irradiation. Adv Exp Med Biol 645: 43-48.

Zhang XJ, Chen S, Huang K-X and Le W-D (2013). Why should autophagic flux be assessed? Acta Pharmacologica Sinica 34(5): 595-599.

Zhang Y, Sowers JR and Ren J (2018). Targeting autophagy in obesity: from pathophysiology to management. Nat Rev Endocrinol 14(6): 356-376.

Zheng X, Dai W, Chen X, Wang K, Zhang W, Liu L and Hou J (2015). Caffeine reduces hepatic lipid accumulation through regulation of lipogenesis and ER stress in zebrafish larvae. J Biomed Sci 22: 105.

Zhu Y, Li YG, Wang JB, Liu SH, Wang LF, Zhao YL, Bai YF, Wang ZX, Li JY and Xiao XH (2015). Causes, Features, and Outcomes of Drug-Induced Liver Injury in 69 Children from China. Gut Liver 9(4): 525-533.

국문 초록

에페드린과 디히드로세라마이드로 유도된 오토파지 손상에 의한 간 독성 기전

서울대학교 대학원

수의병인생물학 및 예방수의학 전공

이 아 영

(지도 교수 : 강 경 선)

비알콜성간질환은 전세계적으로 일반적인 만성 간질환이다. 이러한 간질환을 해결하기 위한 여러 연구가 진행되고 있는데 비알콜성간질환을 발병시키는 기전은 완전히 검증되지 않았다. 본

연구에서는 비알콜성간질환 진행에 있어 간세포에서 산화스트레스와 디히드로세라마이드의 변화에 따른 오토파지 기전이 어떠한 역할을 하는지 밝혀내고자 하였다. 오토파지는 세포가 스트레스 상황에 놓였을 때 손상된 소기관과 단백질들을 제거, 재생하는 과정을 의미한다. 오토파지는 비알콜성간질환에서 세포 상황에 따라 질환이 악화될 수도 완화될 수도 있는 역할을 한다. 그렇기 때문에 오토파지의 기전은 간질환에 대한 새로운 표적 치료가 될 수 있다.

다이어트 한약에 이용되는 마황의 유효성분으로 알려진 에페드린은 최근 많은 연구에서 심장질환, 신경계 등에서 부작용이 보고되고 있다. 뿐만 아니라 에페드린과 같이 많은 약리학적 활성 알칼로이드가 포함된 식물들은 급성 간염을 일으킨다는 보고가 있다. 하지만 많은 임상 보고가 있지만 아직 어떠한 기전으로 간독성을 일으키는지에 대한 연구는 없다. 에페드린은 간세포에서 산화스트레스를 유발하고 미토콘드리아 세포막 에너지를 탈분극시킨다. 전자현미경을 통해 세포 형태를 지켜보았을 때 미토콘드리아의 팽윤이 관찰되었고 시간이 흐름에 따라 autolysosome이 관찰되었다. 또한, 에페드린은 미토콘드리아 활성을 억제하였고 미토콘드리아 복제 수를 감소시켰다. 이러한 미토콘드리아 손상을 회복하기 위하여 미토콘드리아에서 일어나는 오토파지(미토파지)가 일어나게 되는데

오토파지뿐만 아니라 미토파지 관련 유전자들이 증가하게 된다. 하지만 과도한 미토파지가 오토파지의 흐름을 손상하였고 이러한 손상은 세포 사멸을 통한 간독성을 유도하게 된다. 이러한 간독성을 줄이기 위하여 미토파지 관련 유전자인 Parkin siRNA와 항산화제를 이용하여 간독성을 줄일 수 있음을 확인하였다.

스핑고 지질은 다양한 대사 질환에 중요한 역할을 한다. 다양한 스핑고 지질의 기전에 대해서 밝혀져 있지만 디히드로세라마이드의 비알콜성간질환에서의 기전은 아직 밝혀진 바가 없다. 이러한 디히드로세라마이드와 비알콜성간질환에서의 기전을 연구하기 위하여 간세포에 유리지방산을 처리하여 지방증 세포 모델을 만들었고 이를 통해 어떻게 지방증 세포에서 디히드로세라마이드의 증가로 인해 autophagosome의 축적이 일어나는지 확인하였다. 그리고 결과적으로 이러한 오토파지의 변화가 섬유화 반응을 일으키는지 보았다. 먼저 지방증 세포를 지질 분석을 통하여 스핑고지질과 트리글리세롤의 양을 분석하였다. 그리고 다양한 스핑고 지질 합성 억제제를 통하여 오토파지가 어떻게 변화하는지 관찰하였다. 디히드로세라마이드가 지방증 세포에서 증가하였을 때 오토파지 흐름은 손상이 되었고 그에 따른 지방방울(lipid droplet)이 증가함을 관찰하였다. 또한 간성상세포와 간세포의 공생배양(co-culture)을 통해 간섬유화 관련

단백질을 확인하였을 때 간 성상세포 활성화로 인해 섬유화 반응이 유발됨을 확인하였다. 이러한 간 손상을 회복하기 위해 라파마이신을 활용하여 오토파지 흐름을 회복하고자 하였고 이러한 흐름 회복으로 지방 방울이 감소되었고 섬유화 반응 또한 감소됨을 확인하였다. 이러한 결과는 디히드로세라마이드가 오토파지 대사에서 중요한 역할을 함을 알 수 있었고 비알콜성간질환의 진행에서 중요한 기능을 함을 알 수 있었다. 디히드로세라마이드의 조절에 따른 오토파지의 흐름을 원활하게 하는 것이 비알콜성간질환 치료에서 잠재적인 전략적 해결이 될 수 있음을 시사한다.

이러한 연구결과들은 산화스트레스와 디히드로세라마이드의 증가에 따른 오토파지의 흐름의 문제가 비알콜성간질환을 악화시킬 수 있음을 밝혔다. 결과적으로 오토파지의 흐름을 어떻게 조절하느냐에 따라서 비알콜성간질환을 예방할 수도 악화시킬 수도 있음을 알려주었고 이러한 기전을 비알콜성간질환 치료에 적용될 수 있을 것이라 생각한다.

주요어 : 에페드린, 오토파지, Parkin, 미토콘드리아 산화 스트레스, 간섬유화, 간독성, 스핑고지질, 디히드로세라마이드

학 번 : 2012-21547